CHAPTER 4

RESULTS AND DISCUSSION

CHAPTER 4: RESULTS AND DISCUSSION

4.1 Introduction

Six new Schiff bases were prepared from the reaction of mono- and disubstituted salicyaldehydes with 4-phenyl-1,3,5-triazine-2,6-diamine in a 2:1 mole ratio. These bases have substituents with different electronic effects which may modify their physical and chemical properties. The method used was as published in the literature [67]. The general equation for the reaction is shown in **Scheme 4.1.**

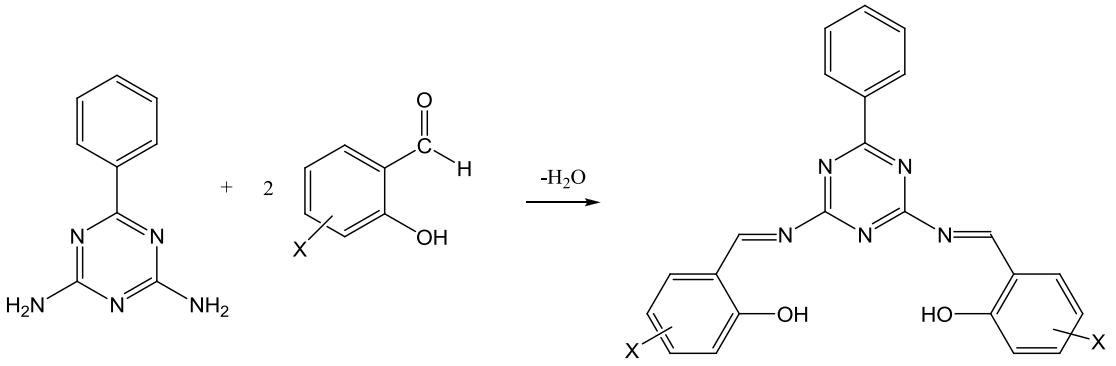

Scheme 4.1 Reaction equation for the preparation of mono- and disubstituted Schiff bases; X = 5-Cl (H_2L1), 5-Br (H_2L2), 5-NO_2 (H_2L3), 3-OH (H_2L4), 4-OH (H_2L5), and 3,5-$(C(CH_3)_3)_2$ (H_2L6)

The chemical and structural formulas of these Schiff bases were ascertained by elemental analysis (CHN), Fourier transform infrared spectroscopy (FT-IR), and ^{1}H- and ^{13}C- nuclear magnetic resonance spectroscopy.

Each of these Schiff bases were then reacted with Ni(II), Cu(II), and Zn(II) acetates to the corresponding complexes (total 18) according to the literature method [69]. These metal ions

were chosen because they have shown good biological activities as antioxidants [4]. The chemical and structural formulas of these complexes were proposed from CHN, FT-IR, and UV-vis, while their thermal stabilities by thermogravimetric analysis (TGA).

4.2 H_2L1 and its Ni(II), Cu(II) and Zn(II) complexes

4.2.1 H_2L1

H_2L1 was obtained as yellow-white powder in good yield (72%) from the reaction shown in **Scheme 4.1** (X = 5-Cl). The results from the CHN elemental analysis are in excellent agreement with the chemical formula, $C_{23}H_{15}O_2N_5Cl_2$.

The **FTIR** spectrum (**Figure 4.1)** shows the characteristics broad peak at 3444 cm^{-1} for intra-molecularly hydrogen bonded -OH group [70], a strong peak due to C=N stretching at 1622 cm^{-1}, another strong peak at 1275 cm^{-1} assigned to C-O phenolic stretching, and peaks in the region 1000 - 1500 cm^{-1} from benzene ring skeletal vibrations. The peak at 825 cm^{-1} is due to aromatic C-H out-of-plane stretching mode. The result strongly supports the formation of the Schiff base.

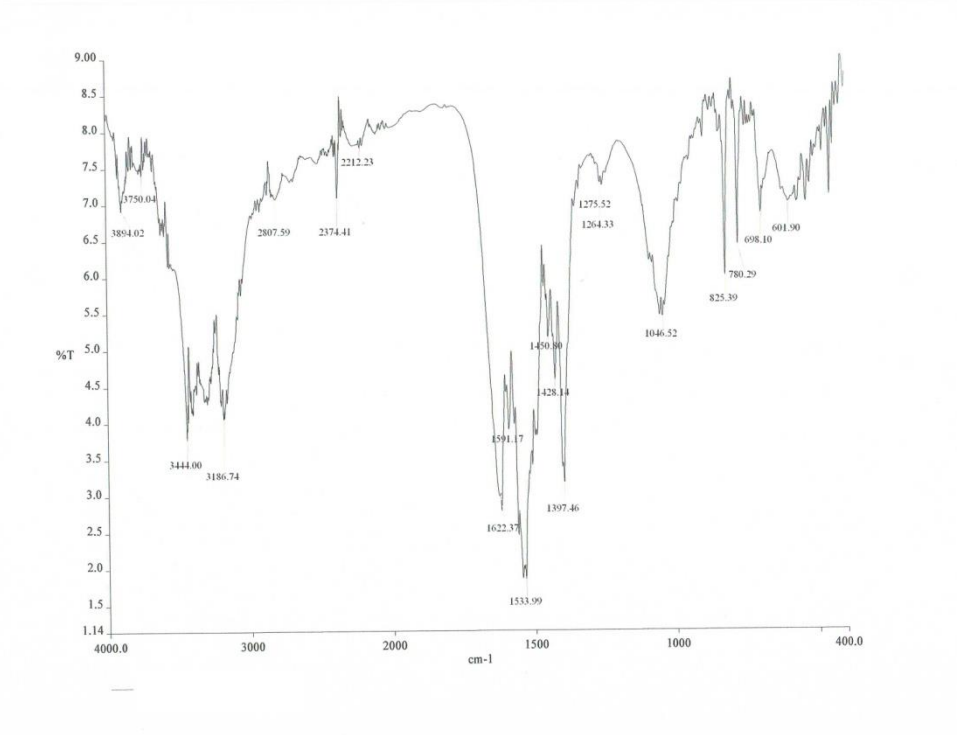

Figure 4.1 FTIR spectrum of H_2L1

The **^{1}H-NMR** spectrum (**Figure 4.2) is** consistent with the expected structural formula of H_2L1: a singlet at 10.19 ppm is due to phenolic hydrogen; a singlet at 8.21 ppm is due to imino hydrogen; and a multiplet in the range 6.72 - 7.70 ppm is due to the aromatic hydrogens. The integration ratio for these hydrogens is 1:1:5.7 respectively (expected ratio = 1:1:5.5), and supports the molecular symmetry for the Schiff base [68].

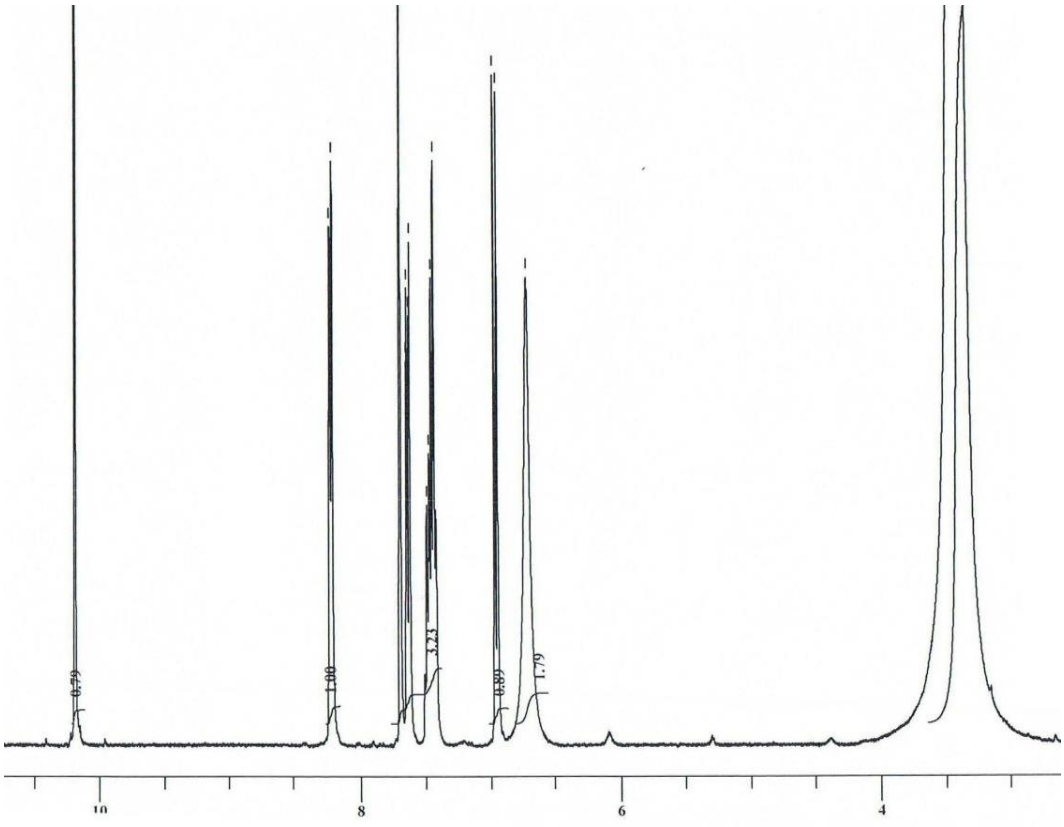

Figure 4.2 ^{1}H-NMR spectrum of H_2L1

The **^{13}C-NMR** spectrum (**Figure 4.3**) shows 12 peaks, assigned as shown in the structure below. However, the expected number of peaks, after taking account of the symmetry of the structure, is 12.

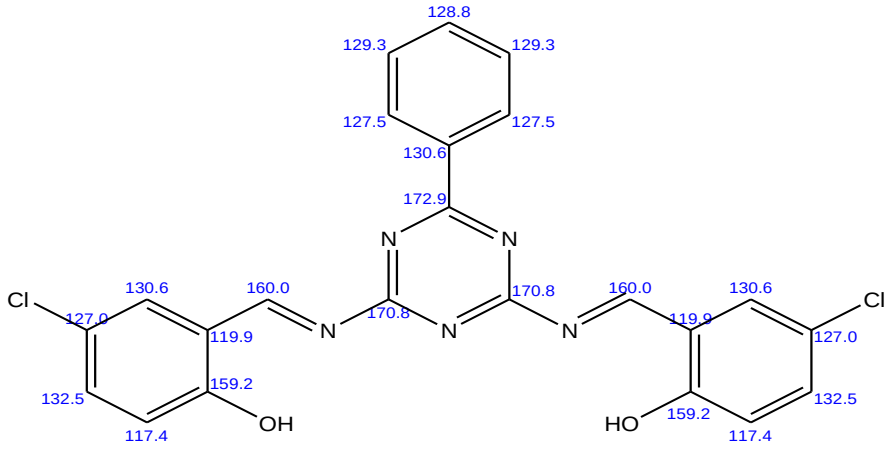

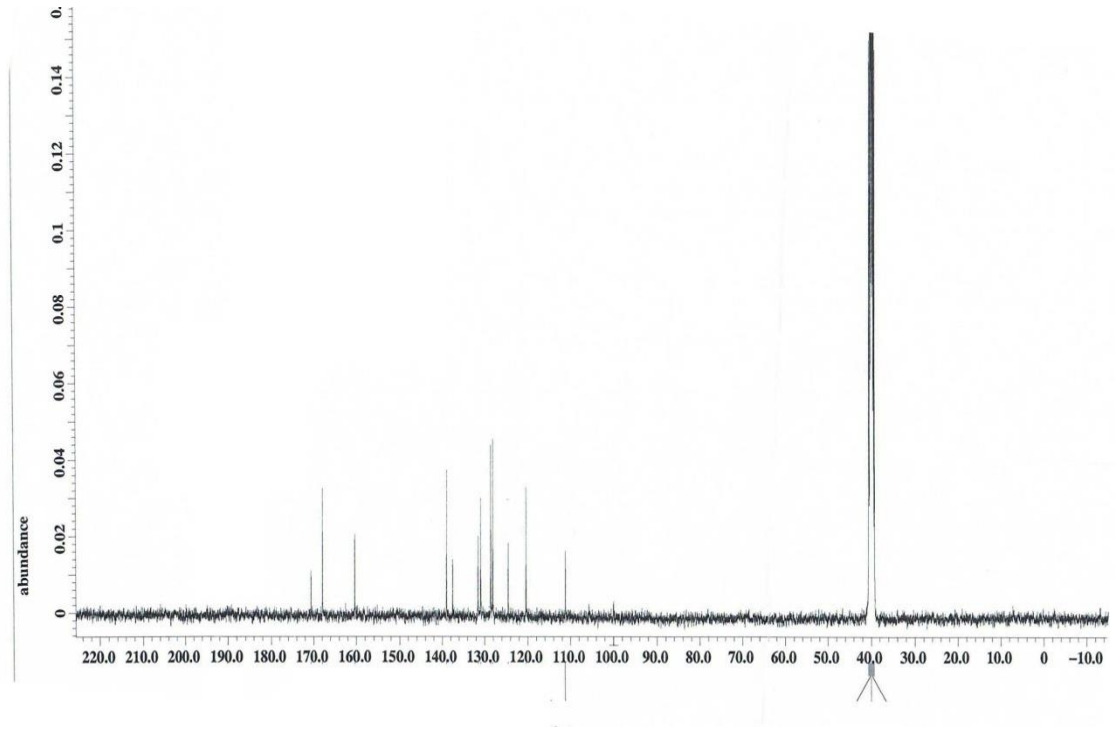

Figure 4.3 ^{13}C-NMR spectrum of H_2L1

The **UV-vis** spectrum of a solution of H_2L1 in DMSO (**Figure 4.4**) shows a high intensity broaden absorption band at about 270 nm ($\varepsilon = 1.1x10^4$ $M^{-1}cm^{-1}$) assigned to π-π^* transition of the aromatic ring. The *n*-π^* transition of the azomethine chromophore is observed as a shoulder at the high intensity peak at about 300 nm ($\varepsilon = 1.4x10^4$ $M^{-1}cm^{-1}$). These values are in agreement with other Schiff bases reported in the literatures. For example, the π-π^* and *n*-π^* transitions were observed 255 nm and 308 nm respectively [71] for $HOC_6H_4CH=NCH_2CH_2CH(CH_2CH_3)N=CHC_6H_4OH$.

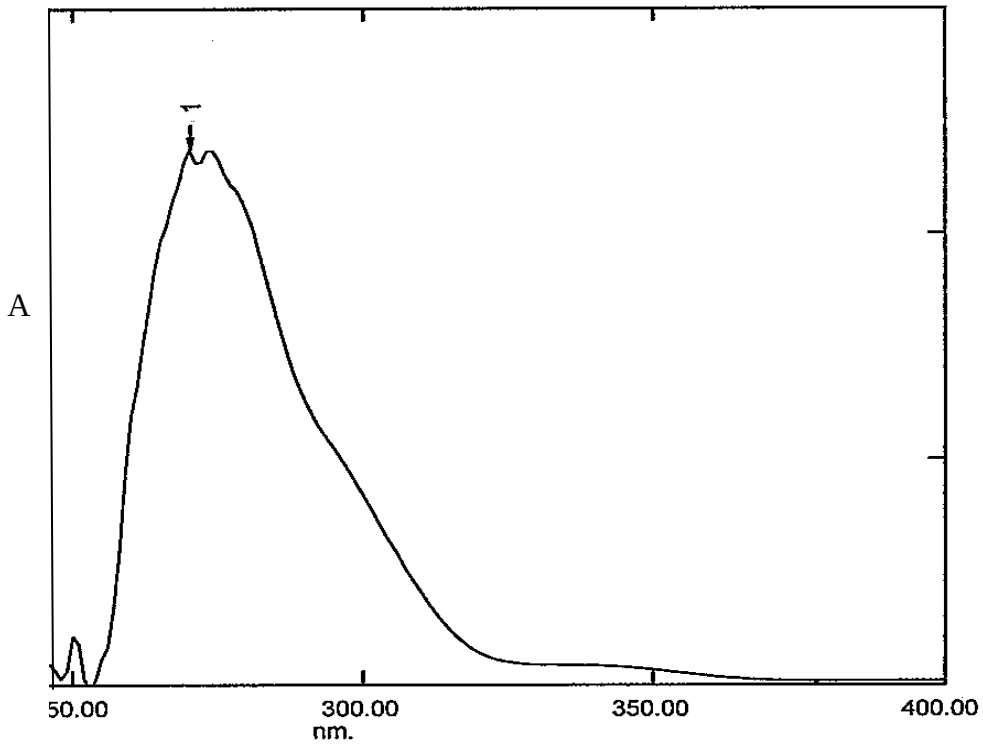

Figure 4.4 UV-vis spectrum of H_2L1 in DMSO

4.2.2 Nickel(II) complex of H_2L1

The nickel(II) complex (NiL1) was obtained as a light-green powder in good yield (62%) in the reaction between H_2L1 and nickel(II) acetate tetrahydrate in presence of triethylamine.

The results from the **CHN** elemental analyses are in excellent agreement with the chemical formula, $[Ni(C_{23}H_{13}O_2N_5Cl_2)(H_2O)_2]$ or $[NiL1(H_2O)_2]$.

The **FTIR** spectrum (**Figure 4.5**) differs from that of H_2L1 (**Figure 4.1**). It is further noted that the -OH peak, observed for H_2L1 at 3444 cm^{-1}, is now observed at 3453 cm^{-1}, and is assigned to coordinated H_2O molecules in agreement with the results from the elemental analyses [72]. The peaks for C=N at 1622 cm^{-1} and C-O at 1275 cm^{-1} observed for H_2L1 are

observed at 1616 cm^{-1} and 1319 cm^{-1} respectively in NiL1.The Ni-O peak is observed at 542 cm^{-1}. These suggest that the phenolic oxygens and imino nitrogens are coordinated to Ni(II).

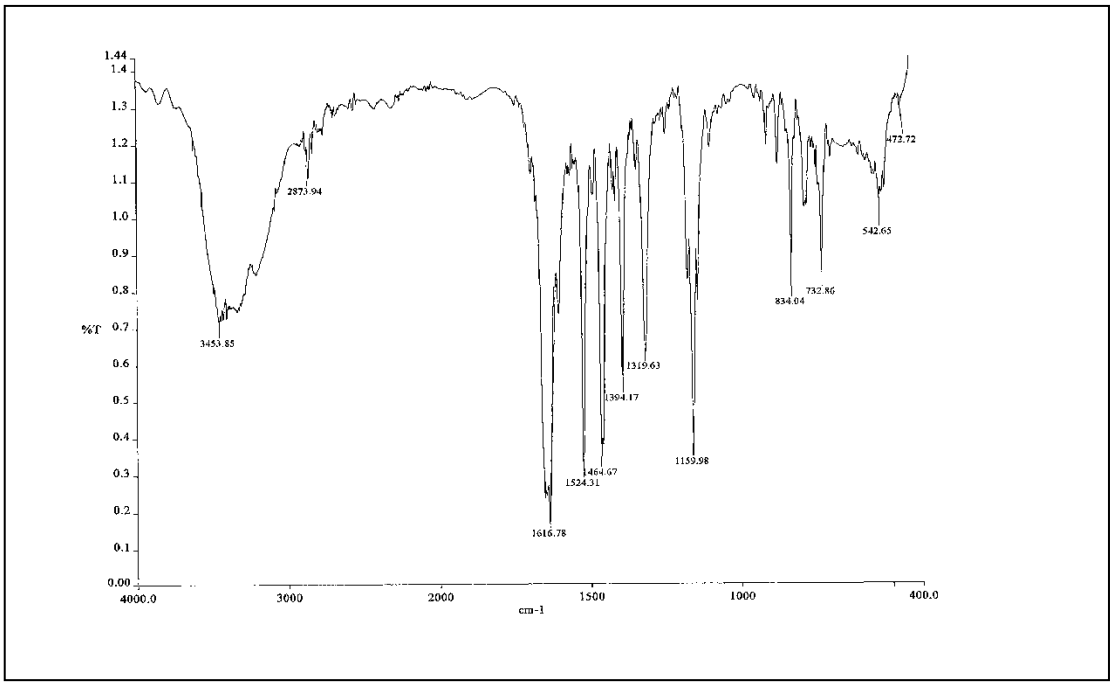

Figure 4.5 FTIR spectrum of [NiL1(H_2O)$_2$]

The **UV-vis** spectrum (**Figure 4.6;** shown as insert) shows weak *d-d* bands 1060 (ε_{max} = 273 $M^{-1}cm^{-1}$), 1010 nm (ε_{max} = 318 $M^{-1}cm^{-1}$), and 899 nm (ε_{max} = 400 $M^{-1}cm^{-1}$). These are consistent with an octahedral configuration at Ni(II), and using the Tanabe-Sugano diagram for d^8 complex (**Figure 4.7**), these bands are assigned to the transitions $^3A_{2g} \rightarrow {}^3T_{2g}$, $^3A_{2g} \rightarrow {}^3T_{1g}(F)$ and $^3A_{2g} \rightarrow {}^3T_{1g}(P)$, respectively, and the value of Δ_o is 13,643 cm^{-1}.

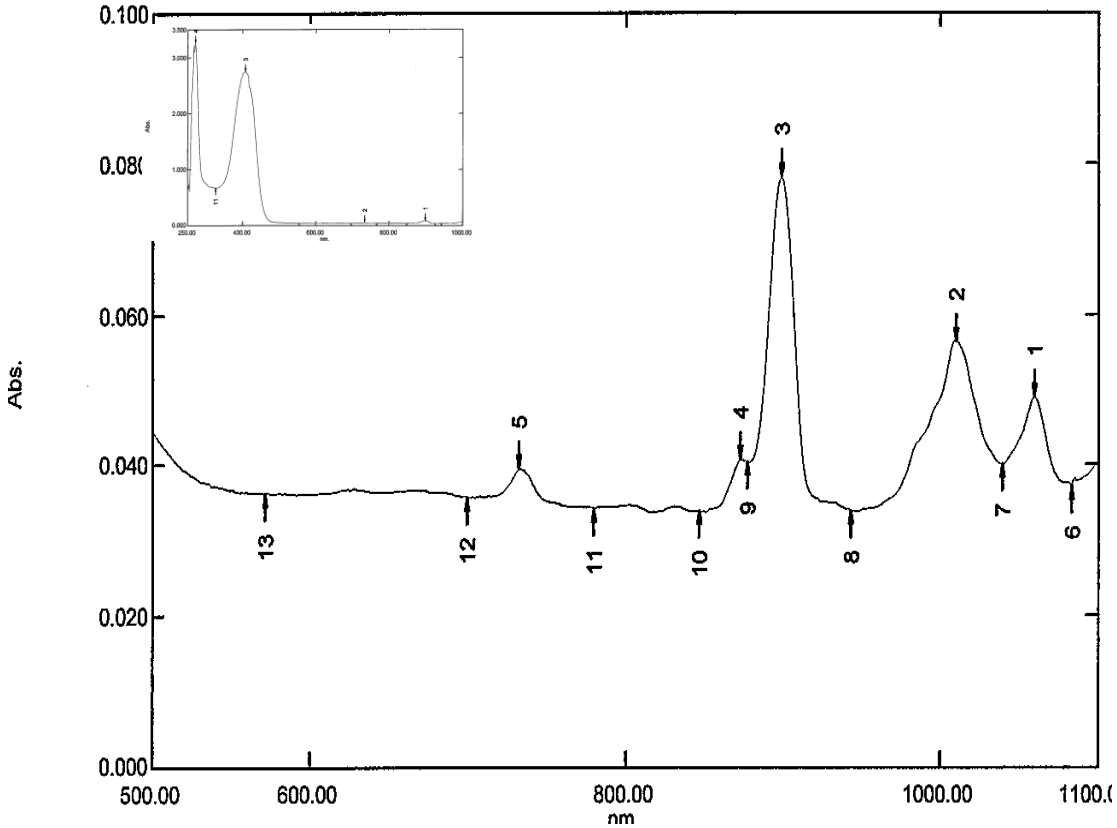

Figure 4.6 UV-vis spectrum of $[NiL1(H_2O)_2]$ in DMSO

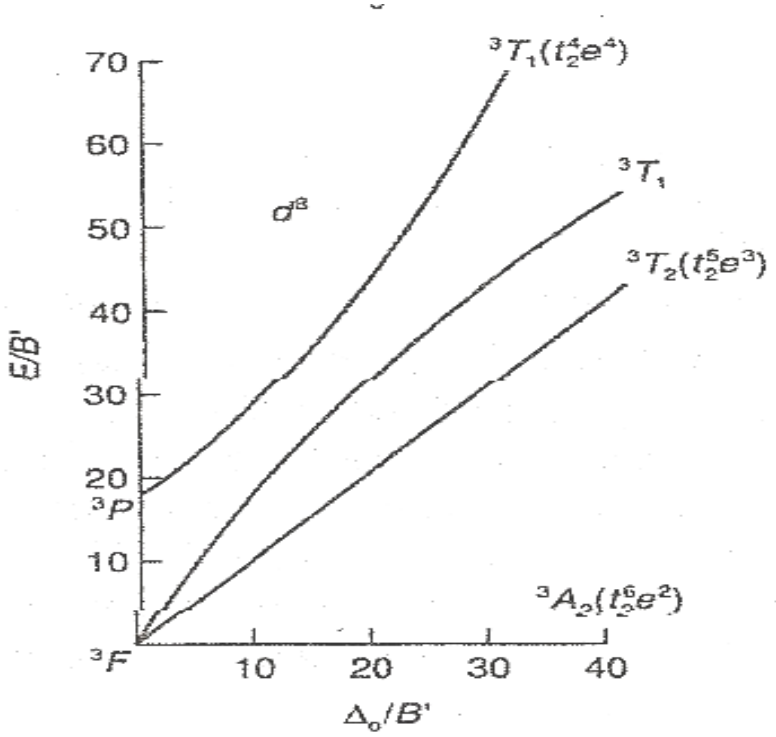

Figure 4.7 Tanabe-Sugano diagram for d^8 octahedral complexes

The peak at 407 nm (ε = 1.5 x 10^4 $M^{-1}cm^{-1}$) is assigned to metal-ligand charge transfer (MLCT) [4]. The spectrum is also compared with that of H_2L1 (**Figure 4.4**). It is noted that the π - π^* band observed for H_2L1 (270 nm) remains almost unshifted in the complex 271 nm(ε = 1.9 x 10^4 $M^{-1}cm^{-1}$). However, the *n* - π^* band may be hidden under the strong MLCT band at 407 nm. Thus, this band is significantly red-shifted from about 300 nm to about 400 nm as a result of complexation to the Ni(II). These results are in agreement with literature result indicating the formation of the complex.

The **TGA** thermogram **(Figure 4.8**), measured from 50^{o}C up to 900^{o}C, shows that the complex was stable up to 245^{o}C [73]. The first weight loss of 5.7% at 125^{o}C corresponds to the loss of coordinated H_2O molecules (expected, 6.5%). The next step represents a total weight loss of 83.6% and is assigned to the decomposition of the ligand (expected, 83.0%). The amount of residue at 840^{o}C is 10.7%. Assuming that the residue is NiO, the expected value is 13.4%, which is within the acceptable experimental error.

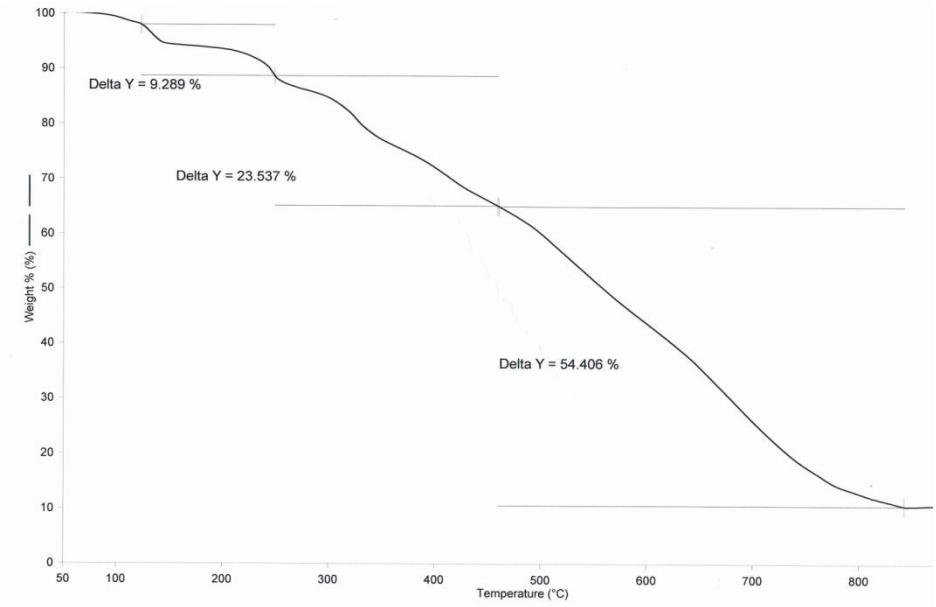

Figure 4.8 TGA for [$NiL1(H_2O)_2$]

Based on the above analytical results, the proposed structure for $[NiL1(H_2O)_2]$ is shown in **Figure 4.9**

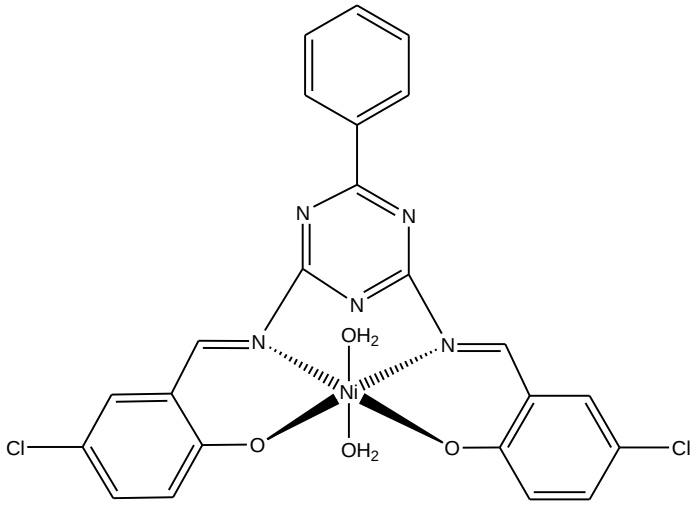

Figure 4.9 Proposed structural formula of $[NiL1(H_2O)_2]$

4.2.3 Copper(II) complex of H_2L1

The copper(II) complex was obtained as a dark-green powder in good yield (71%) in the reaction between H_2L1 and copper(II) acetate monohydrate in presence of triethylamine. The yield is higher than the corresponding Ni(II) complex (62%).

The results from the **CHN** elemental analyses are in excellent agreement with the expected chemical formula $CuC_{23}H_{15}O_3N_5Cl_2$ or $[CuL1(\ H_2O)]$.

The **FTIR** spectrum (**Figure 4.10**) shows the expected functional groups as previously discussed for the corresponding Ni(II) complex (**Figure 4.5**). The C=N and C-O peaks for $[CuL1].H_2O$ are at 1616 cm^{-1} and 1317 cm^{-1} respectively. These are almost similar to those of the corresponding Ni(II) complex, suggesting similar bond strength. The Cu-O peak is observed at 565 cm^{-1}, which is higher than that of Ni-O peak (542 cm^{-1}), indicating a stronger M-O bond in the copper(II) complex.

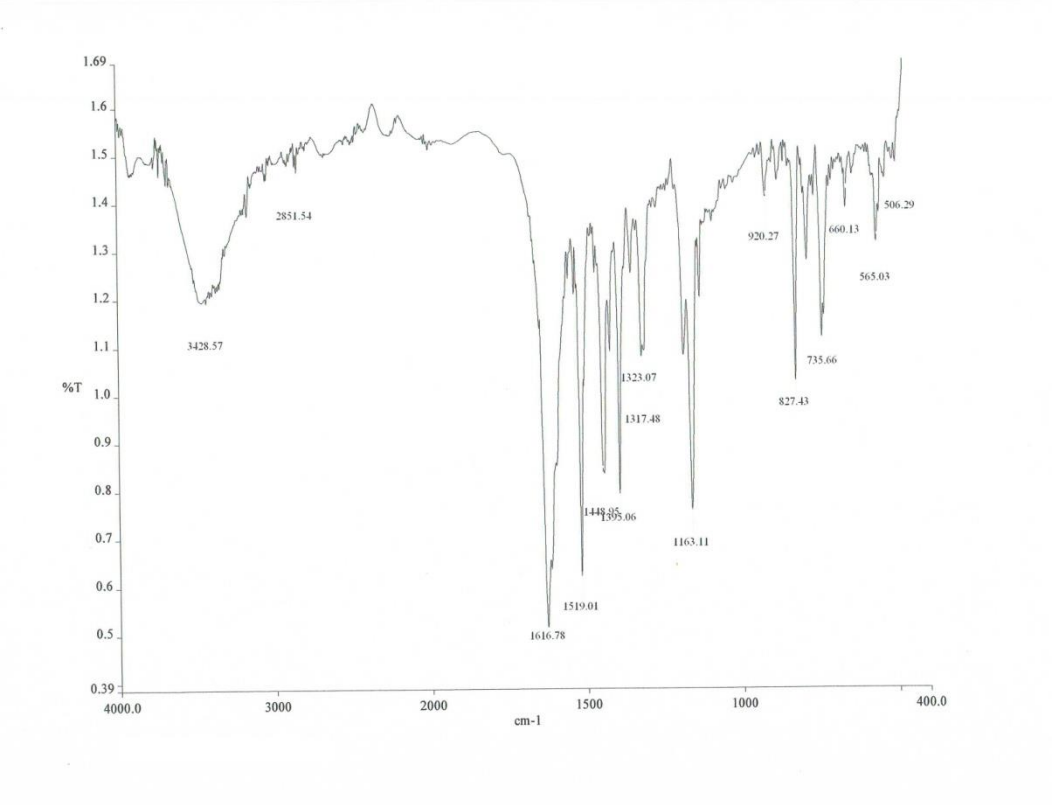

Figure 4.10 FTIR spectrum of [CuL1(H_2O)]

The **UV-vis** spectrum (**Figure 4.11**) shows a broad *d-d* peak at 700 nm (ε_{max} = 200 $M^{-1}cm^{-1}$). Thus, [CuL1(H_2O)] is a mononuclear square pyramidal complex [69]. The π - π^* and MLCT bands are at 268 nm(ε = 1.7x10^4 $M^{-1}cm^{-1}$) and 396 nm(ε = 0.8x10^4 $M^{-1}cm^{-1}$) respectively, which are almost the same as for the corresponding Ni(II) complex (271 nm, 407 nm), and may be similarly explained.

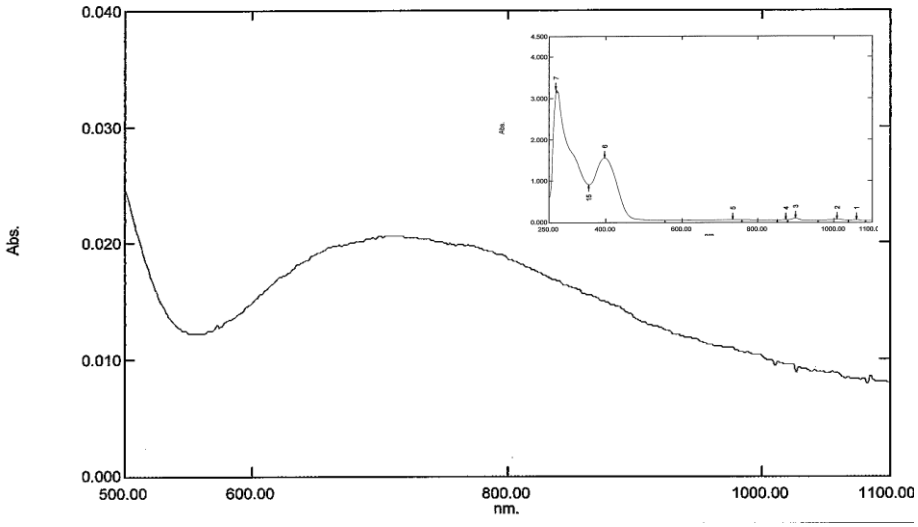

Figure 4.11 UV-vis spectrum of [CuL1(H_2O)]

The **TGA** thermogram **(Figure 4.12**), measured from 50^oC up to 900^oC, shows that the complex was stable up to 255^oC. Thus, [CuL1(H_2O)] is more stable than [NiL1($H_2O)_2$] (245^oC). This is consistent with the stronger Cu-O bond compared to Ni-O bond, from FTIR.

The first weight loss of 4.9% at 75^oC corresponds to the loss of coordinated H_2O molecule (expected, 3.3%). The next step represents a total weight loss of 78.6% and is assigned to the decomposition of the ligand (expected, 85.4%). The amount of residue at about 670^oC is 16.5%. Assuming that the residue is CuO, the expected value is 14.6%. The result suggests incomplete combustion of the complex. Thus, the thermal properties of [CuL1(H_2O)] is different from that of [NiL1($H_2O)_2$] [73].

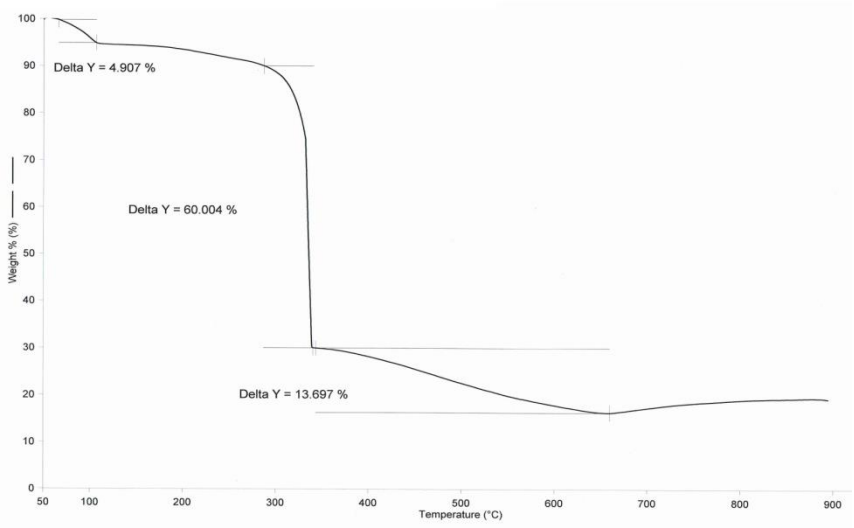

Figure 4.12 TGA for [CuL1(H_2O)]

Based on the above analytical results, the proposed structure for [CuL1(H_2O)] is shown in **Figure 4.13.**

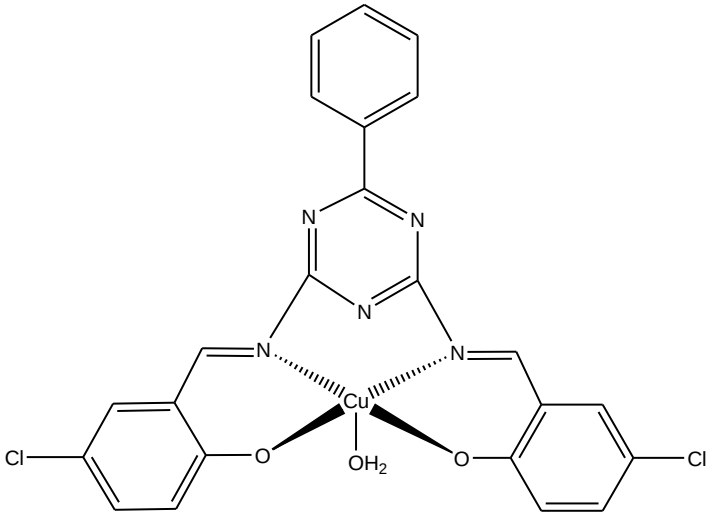

Figure 4.13 Proposed structural formula of [CuL1(H_2O)]

.

4.2.4 Zinc(II) complex of H_2L1

The zinc(II) complex was obtained as a yellow powder in good yield (79%) in the reaction between H_2L1 and zinc(II) acetate dihydrate in presence of triethylamine. The yield is slightly higher than the corresponding Ni(II) complex (62%) and Cu(II) complex (71%).

The results from the **CHN** elemental analyses are in excellent agreement with the expected chemical formula $ZnC_{23}H_{17}O_4N_5Cl_2$ or $[ZnL1].2H_2O$.

The **FTIR** spectrum of $[ZnL1].2H_2O$ (**Figure 4.14**) shows the presence of all the expected functional groups. The wavenumbers of C=N (1616 cm^{-1}) and C-O (1314 cm^{-1}) groups are almost the same as for $[CuL1(H_2O)]$ (1616 cm^{-1} and 1317 cm^{-1} respectively.

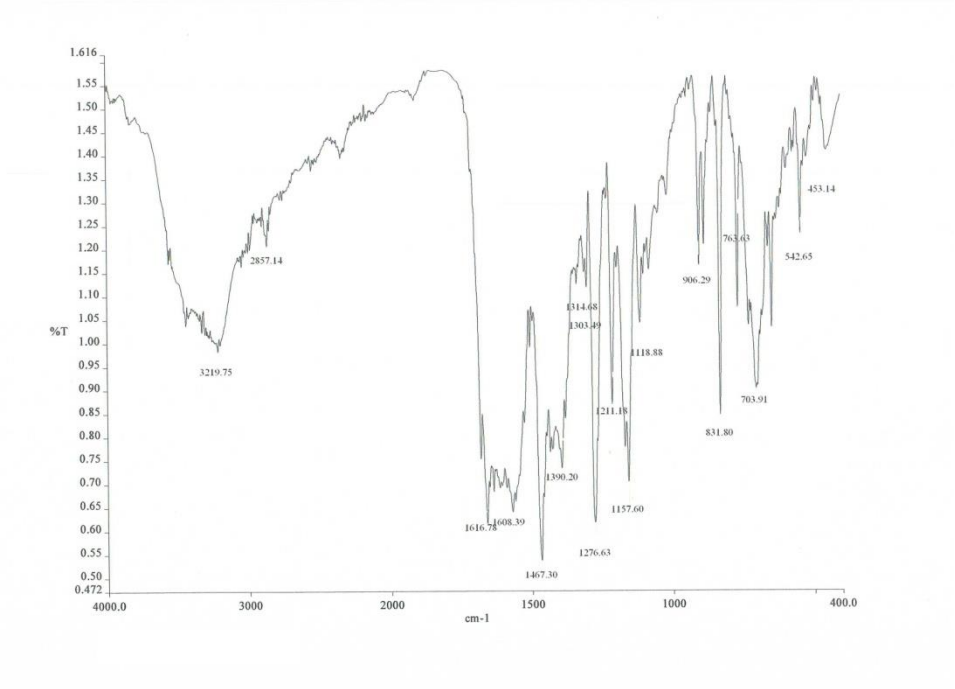

Figure 4.14 FTIR spectrum of $[ZnL1].2H_2O$

The **UV-vis** spectrum of $[ZnL1].2H_2O$ (**Figure 4.15**) shows that the MLCT and π - π^*peaks 390 nm ($\varepsilon = 1.4x10^4$ $M^{-1}cm^{-1}$) and 272 nm($\varepsilon = 2x10^4$ $M^{-1}cm^{-1}$) are at almost the same

energy as the corresponding peaks for [CuL1].H_2O (396 nm, 268 nm; **Figure 4.11**). Thus, both metal ions have insignificant effect on the electronic transitions of the organic moiety. The MLCT peak is normally observed from 348 nm to 323 nm for Zn(II) complexes, involving electronic transitions from the full *d* orbitals of the metal ion ($3d^{10}$) to antibonding orbitals of the ligand [75].

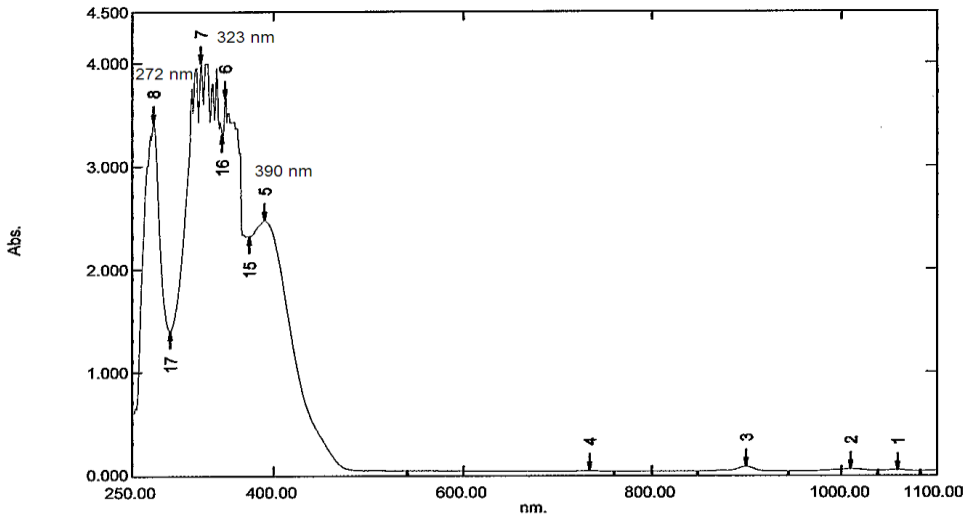

Figure 4.15 UV-vis spectrum of [ZnL1].$2H_2O$

The **TGA** thermogram **(Figure 4.16)**, measured from 50^oC up to 900^oC, shows that the complex was stable up to 228^oC. Thus, it is less thermally stable compared to [CuL1(H_2O)] (255^oC).

The first weight loss of 5.5% at 130^oC corresponds to the loss of coordinated H_2O molecules (expected, 6.3%). The next step represents a total weight loss of 81.3% and is assigned to the decomposition of the ligand (expected, 82.4%). The amount of residue at 780^oC is 13.2%. Assuming that the residue is ZnO, the expected value is 14.4%, which is within the acceptable experimental error.

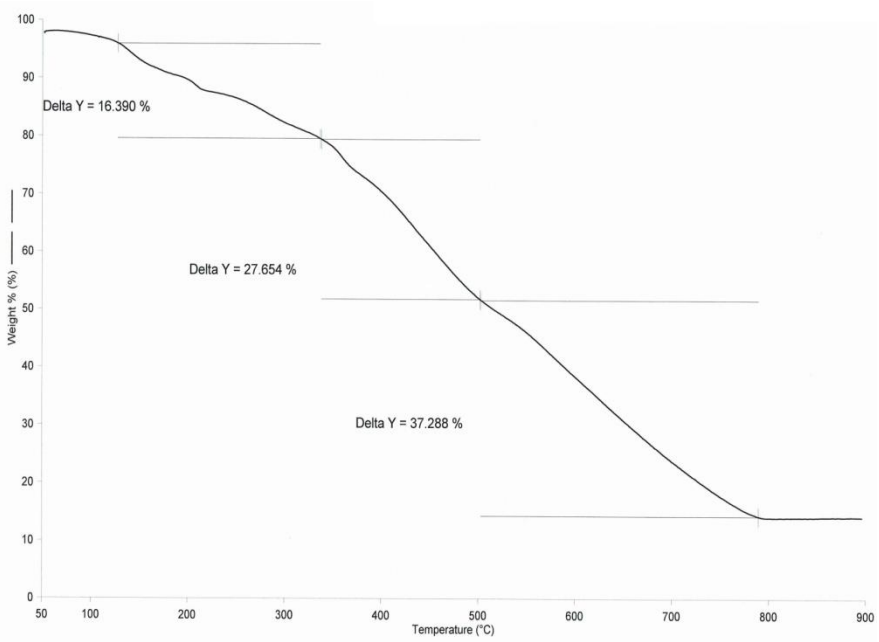

Figure 4.16 TGA for [ZnL1].2H_2O

Based on the above analytical results, and on the knowledge that Zn(II) prefers tetrahedral geometry, the proposed structure for [ZnL1].2H_2O is shown in **Figure 4.17.**

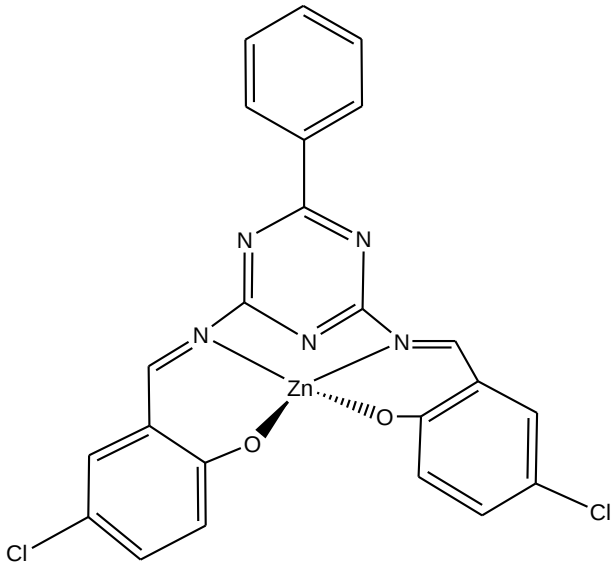

Figure 4.17 Proposed structural formula of [ZnL1].2H_2O (the solvate H_2O is not shown)

4.3 H_2L2 and its Ni(II), Cu(II) and Zn(II) complexes

4.3.1 H_2L2

H_2L2 was obtained as yellow-white powder in good yield (82%) from the reaction shown in **Scheme 4.1** (X = 5-Br). The yield is higher than H_2L1 (72%), indicating lower solubility in ethanol.

The results from the CHN elemental analysis are in excellent agreement with the chemical formula, $C_{23}H_{15}O_2N_5Br_2$.

The **FTIR** spectrum (**Figure 4.18)** shows the presence of all of the expected functional groups at almost the same wavenumbers as discussed for H_2L1. Thus, replacing Cl has no significant effect on the bond strengths of C=N and C-O functional groups of the Schiff base.

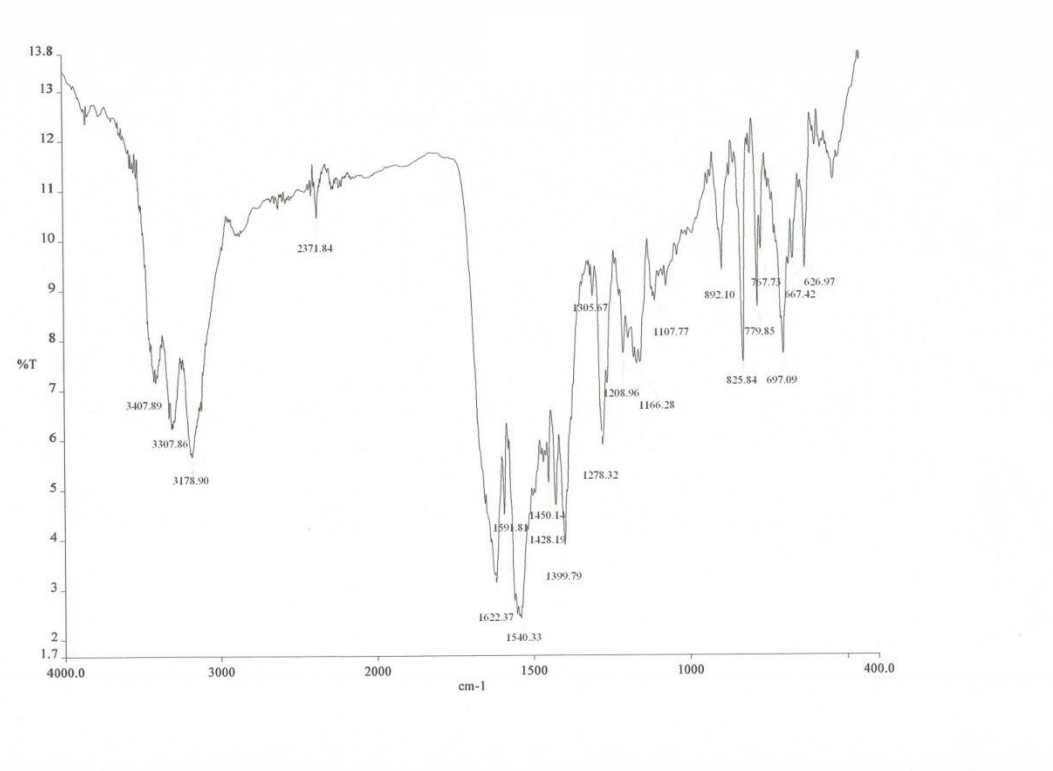

Figure 4.18 FTIR spectrum of H_2L2

The **^{1}H-NMR** spectrum (**Figure 4.19)** is consistent with the expected structural formula of H_2L2: a singlet at 10.21 ppm for the phenolic hydrogen; a singlet at 8.25 ppm for the imino hydrogen; and a multiplet in the range 6.74 - 7.72 ppm for the aromatic hydrogens. The integration ratio for these hydrogens is 1:1:5.6 respectively (expected ratio = 1:1:5.5)[77]. The results support the molecular symmetry for the Schiff base, and indicate insignificant electronic effects when Cl (H_2L1) is replaced by Br (H_2L2).

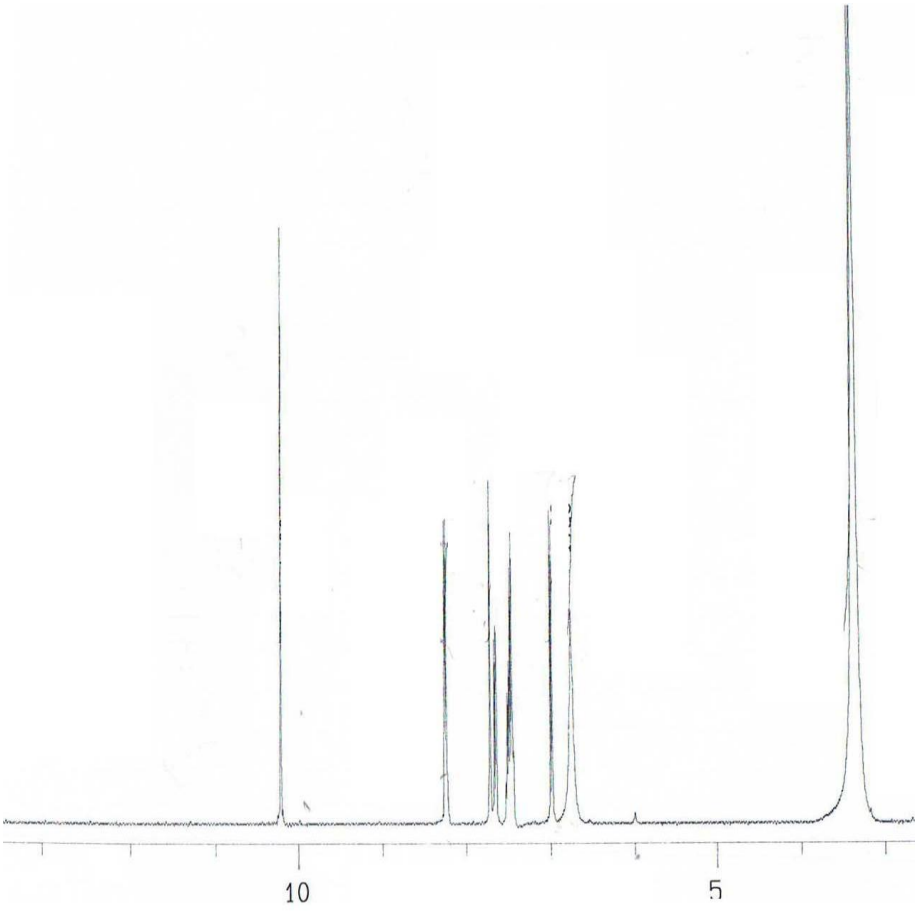

Figure 4.19 ^{1}H-NMR spectrum of H_2L2

The **^{13}C-NMR** spectrum (**Figure 4.20**) shows 12 peaks, assigned as shown in the structure below. However, the expected number of peaks, after taking account of the symmetry

of the structure, is 12. Thus, compared to H_2L1, Br in H_2L2 has shifted the chemical shift of the carbon atom directly bonded to it to lower energy (more shielded). At the same time, the two *ortho-* carbon atoms to it were deshielded, and insignificant effects on the other carbon atoms.

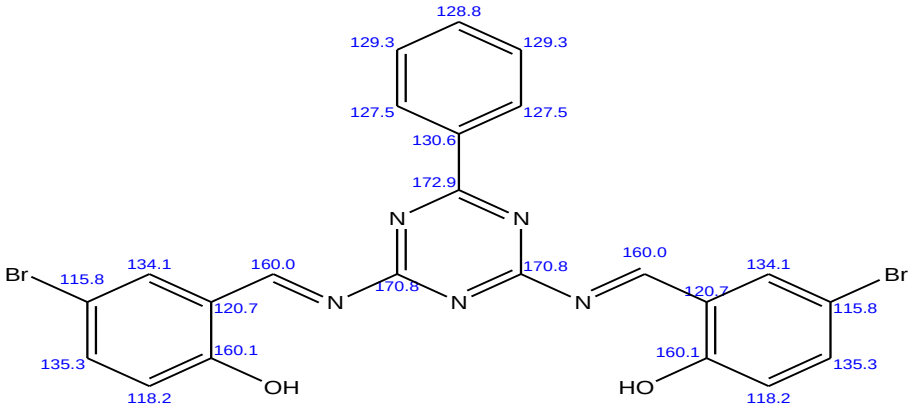

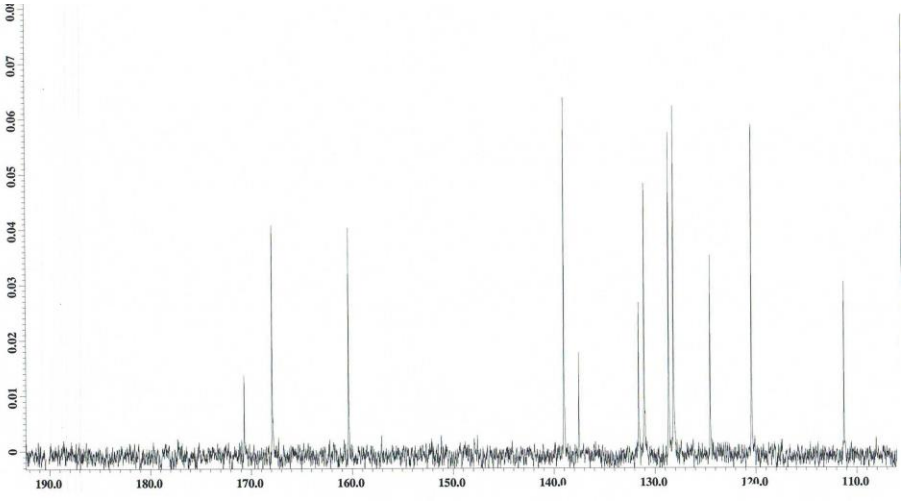

Figure 4.20 ^{13}C-NMR spectrum of H_2L2

The **UV-vis** spectrum of a solution of H_2L2 in DMSO (**Figure 4.21**) shows a high intensity broaden absorption band at about 279 nm ($\varepsilon = 1.5x10^4$ $M^{-1}cm^{-1}$) assigned to π - π^* transition of the aromatic ring. The *n* - π^* transition of the azomethine chromophore is observed

as a shoulder at the high intensity peak at about 345 nm (ε = 1.6x10^4 M^{-1}cm^{-1}) [78]. Thus, compared to H_2L1 (270 nm, 378 nm), there is no significant effect for the π - π^* transition, while the *n* - π^* transition was shifted to higher energy when Cl was replaced by Br.

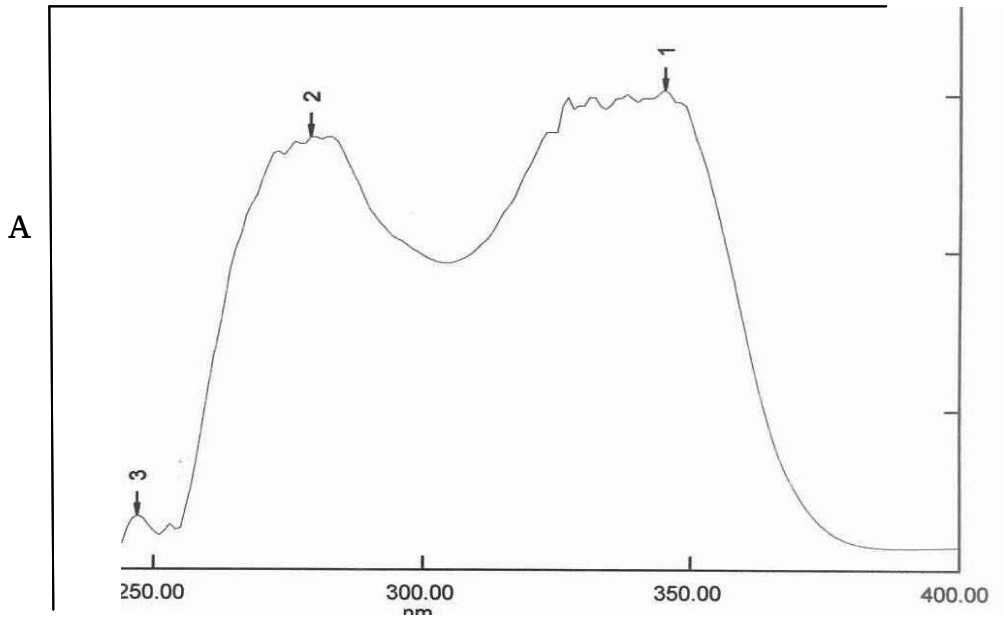

Figure 4.21 UV-vis spectrum of H_2L2 in DMSO

4.3.2 Nickel(II) complex of H_2L2

The nickel(II) complex was obtained as a light-green powder in good yield (76%) in the reaction between H_2L2 and nickel(II) acetate tetrahydrate in presence of triethylamine. The yield is higher than [NiL1(H_2O)2] (62%), indicating lower solubility in ethanol.

The results from the **CHN** elemental analyses are in excellent agreement with the chemical formula, [Ni($C_{23}H_{13}O_2N_5Br_2$)(H_2O)$_2$] or [NiL2(H_2O)$_2$].

The **FTIR** spectrum (**Figure 4.22**) differs from that of H_2L2 (**Figure 4.18**). It is further noted that the -OH peak, observed for H_2L2 at 3407 cm^{-1}, is now observed at 3421 cm^{-1}, and is

assigned to coordinated H_2O molecules in agreement with the results from the elemental analyses [74]. The peaks for C=N at 1622 cm^{-1} and C-O at 1378 cm^{-1} observed for H_2L2 are observed at 1617 cm^{-1} and 1321 cm^{-1} respectively in $[NiL2(H_2O)_2]$. The Ni-O peak is observed at 537 cm^{-1}. These suggest that the phenolic oxygens and imino nitrogens are coordinated to Ni(II). Also, it is noted that the strengths of C=N and C-O bonds are similar for $[NiL2(H_2O)_2]$ (1617 cm^{-1}; 1321cm^{-1} respectively) compared to those of $[NiL1(H_2O)_2]$ (1616 cm^{-1}; 1319 cm^{-1} respectively).

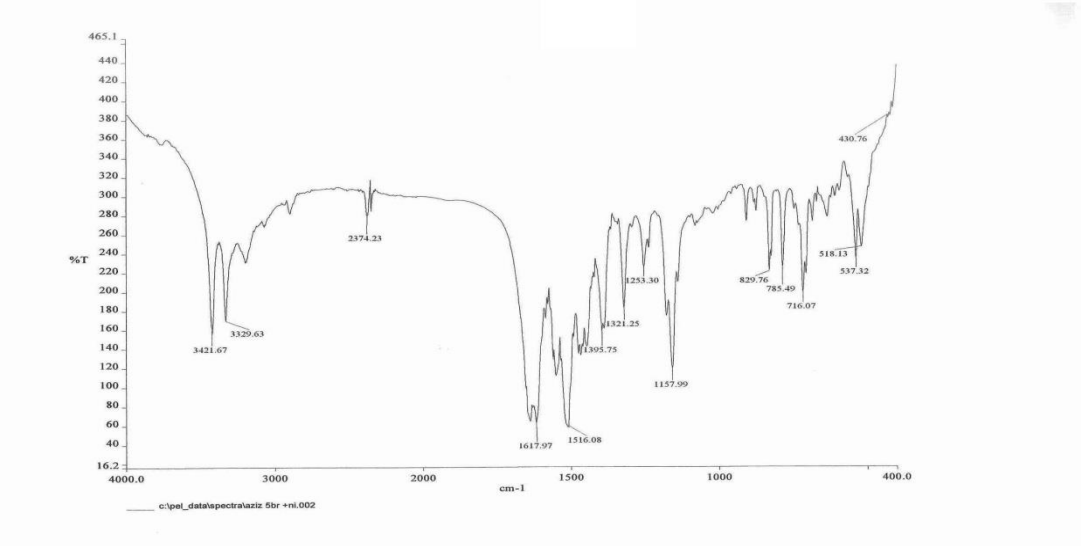

Figure 4.22 FTIR spectrum of $[NiL2(H_2O)_2]$

The **UV-vis** spectrum of $[NiL2(H_2O)_2]$ (**Figure 4.23**) shows *d-d* bands at 1060 nm (ε_{max} = 298 $M^{-1}cm^{-1}$), 1010 nm (ε_{max} = 357 $M^{-1}cm^{-1}$), and 899 nm (ε_{max} = 500 $M^{-1}cm^{-1}$). These are consistent with an octahedral configuration at Ni(II), and these bands are similarly assigned as for $[NiL1(H_2O)_2]$. The peak at 405 nm ($\varepsilon = 1.9 \times 10^4$ $M^{-1}cm^{-1}$) is assigned to metal-ligand charge transfer (MLCT).

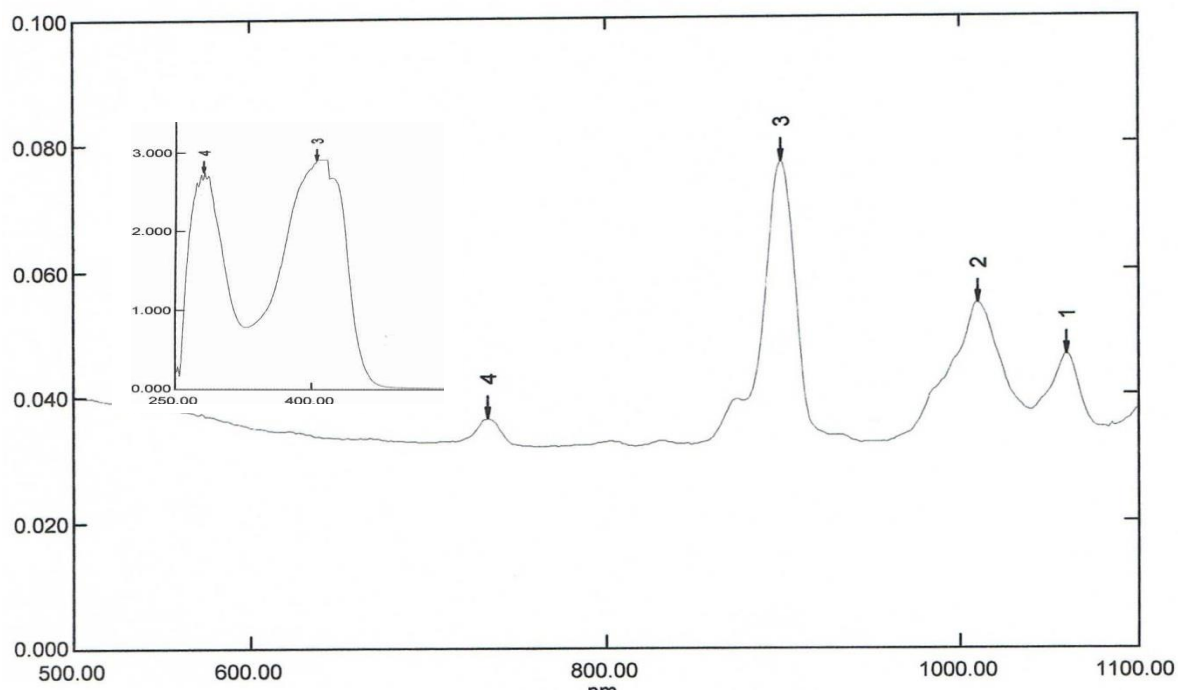

Figure 4.23 UV-vis spectrum of [NiL2(H_2O)$_2$] in DMSO

The **TGA** thermogram **(Figure 4.24)**, measured from 50^{o}C up to 900^{o}C, shows that the complex was stable up to 250^{o}C. Thus, it is slightly similar themally stable for [NiL1(H_2O)$_2$] (245^{o}C)**.** Thus, substituting Br for Cl at the 5-position of the phenolic ring has no significant effect on the structure of the complex.

The first weight loss of 2.8% at 125^{o}C corresponds to the loss of coordinated H_2O molecules (expected, 5.5%). The next step represents a total weight loss of 88.0% and is assigned to the decomposition of the ligand (expected, 85.6%). The amount of residue at temperatures above 870^{o}C is 9.2%. Assuming that the residue is NiO, the expected value is 11.5%, which is within the acceptable experimental error.

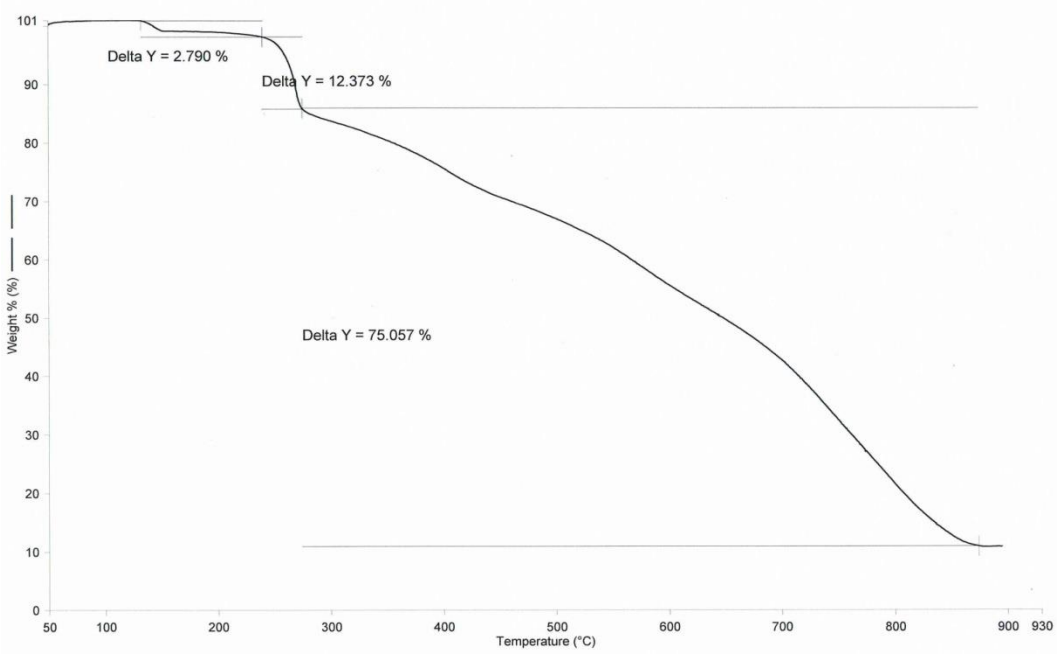

Figure 4.24 TGA for [NiL2(H_2O)$_2$]

Based on the above analytical results, the proposed structure for [NiL2(H_2O)$_2$] is shown in **Figure 4.25.** Thus, substituting Br for Cl at the 5-position of the phenolic ring has no significant effect on the structure of the complex.

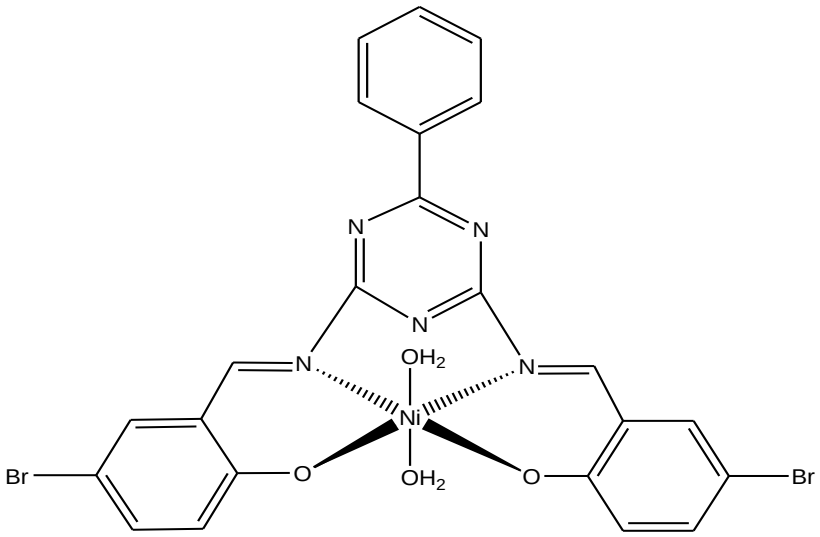

Figure 4.25 Proposed structural formula of [NiL2(H_2O)$_2$]

4.3.3 Copper(II) complex of H_2L2

The copper(II) complex was obtained as a dark-green powder in good yield (70%) in the reaction between H_2L2 and copper(II) acetate monohydrate in presence of triethylamine. The yield is similar to $[CuL1(H_2O)]$ (71%), indicating similar solubility in ethanol.

The results from the **CHN** elemental analyses are in excellent agreement with the expected chemical formula $CuC_{23}H_{15}O_3N_5Br_2$ or $[CuL2(H_2O)]$.

The **FTIR** spectrum (**Figure 4.26**) shows the expected functional groups as previously discussed for $[CuL1(H_2O)]$ (**Figure 4.10**). The C=N and C-O peaks for $[CuL2(H_2O)]$ are at 1616 cm^{-1} and 1320 cm^{-1} respectively. These are almost similar to those of $[CuL1(H_2O)]$ (1616 cm^{-1} and 1317 cm^{-1}), suggesting similar bond strength.

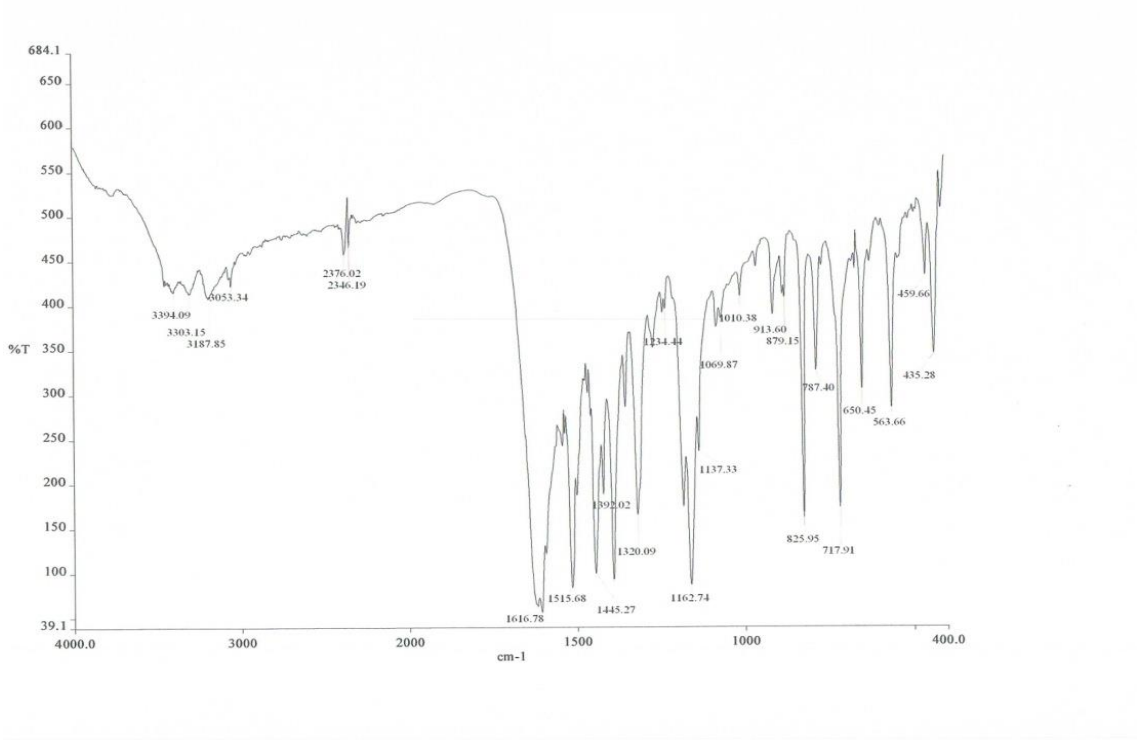

Figure 4.26 FTIR spectrum of $[CuL2(H_2O)]$

The **UV-vis** spectrum (**Figure 4.27**) shows a broad *d-d* peak at 699 nm (ε_{max} = 313 $M^{-1}cm^{-1}$). Thus, [CuL2(H_2O)] is a mononuclear square pyramidal complex [71]. The MLCT band is at 403 nm(ε_{max} = $1.9x10^4$ $M^{-1}cm^{-1}$), which is almost the same as for the corresponding and [CuL1(H_2O)], may be similarly explained.

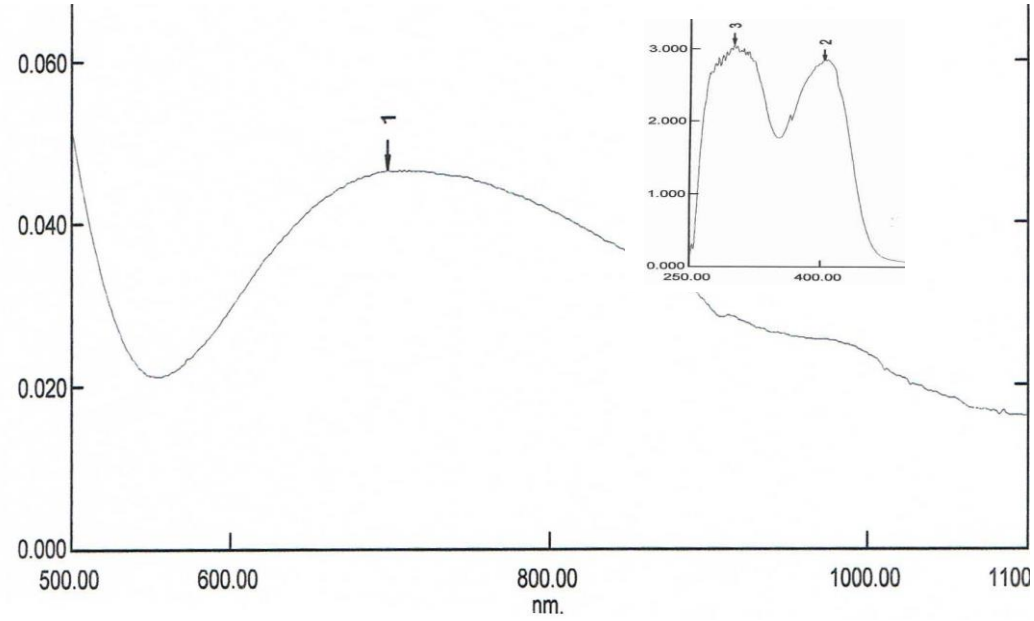

Figure 4.27 UV-vis spectrum of [CuL2(H_2O)]

The **TGA** thermogram **(Figure 4.28)**, measured from 50°C up to 900°C, shows that the complex was stable up to 250°C. Thus, it is as themally stable as [CuL1(H_2O)] (255°C). Thus, substituting Br for Cl at the 5-position of the phenolic ring has no significant effect on the structure of the complex.

The first weight loss of 4.0% at 122°C corresponds to the loss of coordinated H_2O molecules (expected, 2.8%). The next step represents a total weight loss of 86.4% and is assigned to the decomposition of the ligand (expected, 87.4%). The amount of residue at 865°C

is 9.6%. Assuming that the residue is CuO, the expected value is 12.5%, which is within the acceptable experimental error.

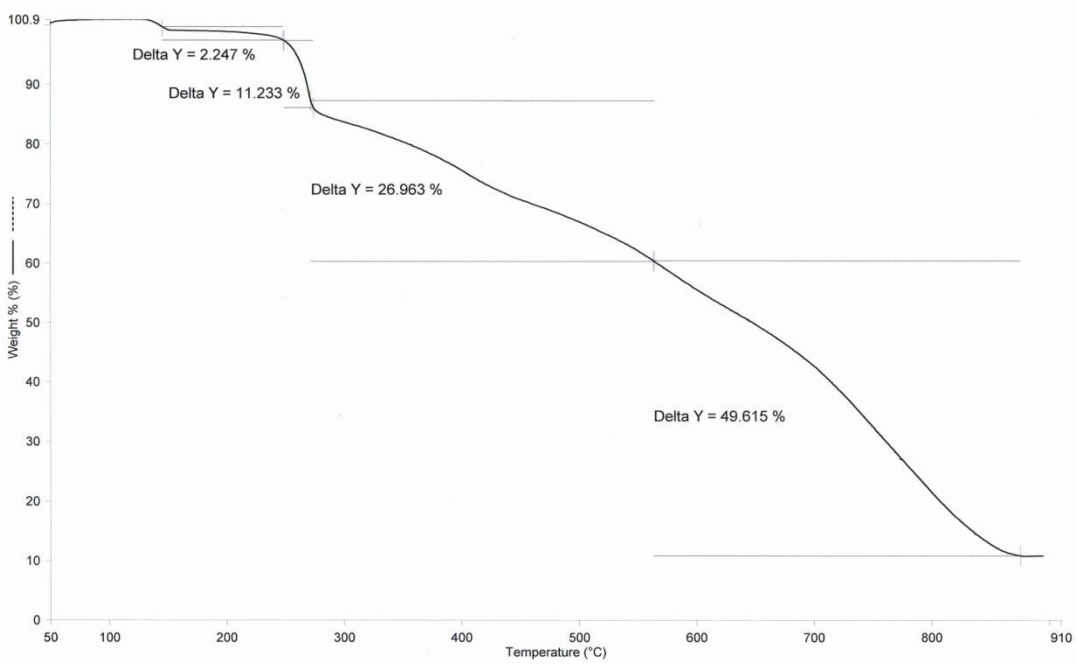

Figure 4.28 TGA for[CuL2].H_2O

Based on the above analytical results, the proposed structure for [CuL2(H_2O)] is shown in **Figure 4.29.** Thus, substituting Br for Cl at the 5-position of the phenolic ring has no significant effect on the structure of the complex.

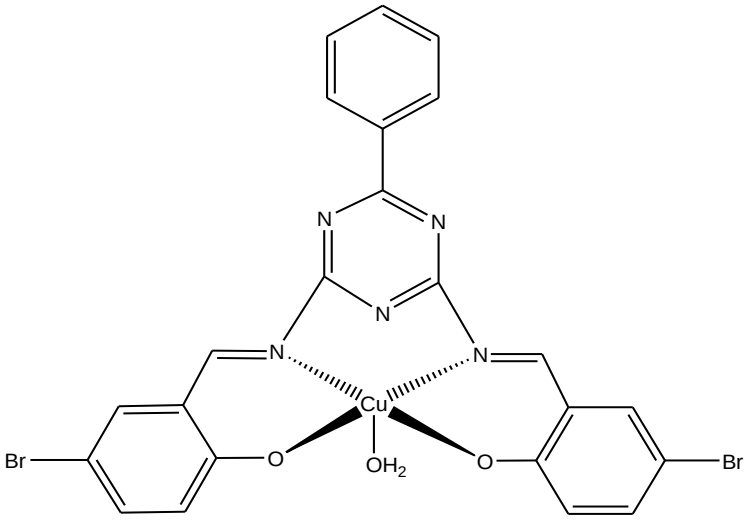

Figure 4.29 Proposed structural formula of [CuL2(H_2O)]

4.3.4 Zinc(II) complex of H_2L2

The zinc(II) complex was obtained as a yellow powder in good yield (74%) in the reaction between H_2L2 and zinc(II) acetate dihydrate in presence of triethylamine. The yield is similar to that of [ZnL1].2H_2O (70%), suggesting similar solubility in ethanol.

The results from the **CHN** elemental analyses are in excellent agreement with the expected chemical formula $ZnC_{23}H_{17}O_4N_5Br_2$ or [ZnL2].2H_2O.

The **FTIR** spectrum of [ZnL2].2H_2O (**Figure 4.30**) shows the presence of all the expected functional groups. The wavenumbers of C=N (1617 cm^{-1}) and C-O (1315 cm^{-1}) groups are almost the same as for [ZnL1].2H_2O (1616 cm^{-1} and 1314 cm^{-1} respectively. Thus, the C=N and C-O bond strengths are similar in both complexes.

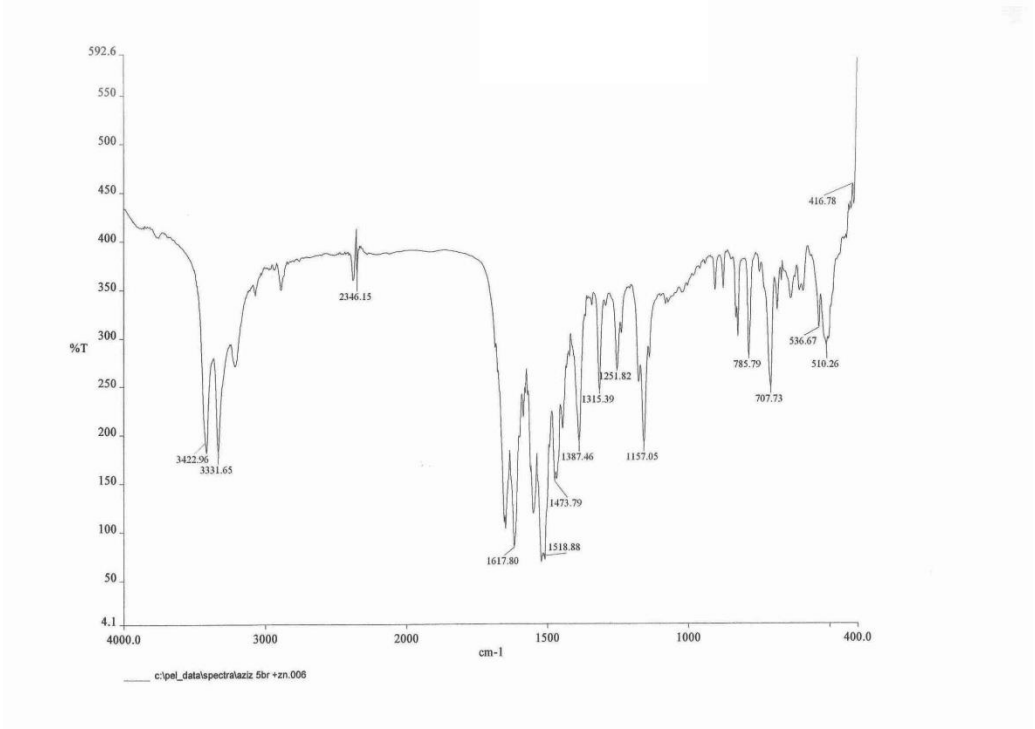

Figure 4.30 FTIR spectrum of [ZnL2].2H_2O

The **UV-vis** spectrum of [ZnL2].2H_2O (**Figure 4.31**) shows that the MLCT and π - π^* peaks 391 nm(ε_{max} = 1.3x10^4 $M^{-1}cm^{-1}$) and 279 nm(ε_{max} = 1.8x10^4 $M^{-1}cm^{-1}$) are at almost the same energy as the corresponding peaks for [ZnL1].2H_2O (390 nm, 272 nm; **Figure 4.15**). Thus, substituting Br for Cl at the 5-position of the phenolic ring has no significant effect on the electronic transitions of the organic moiety.

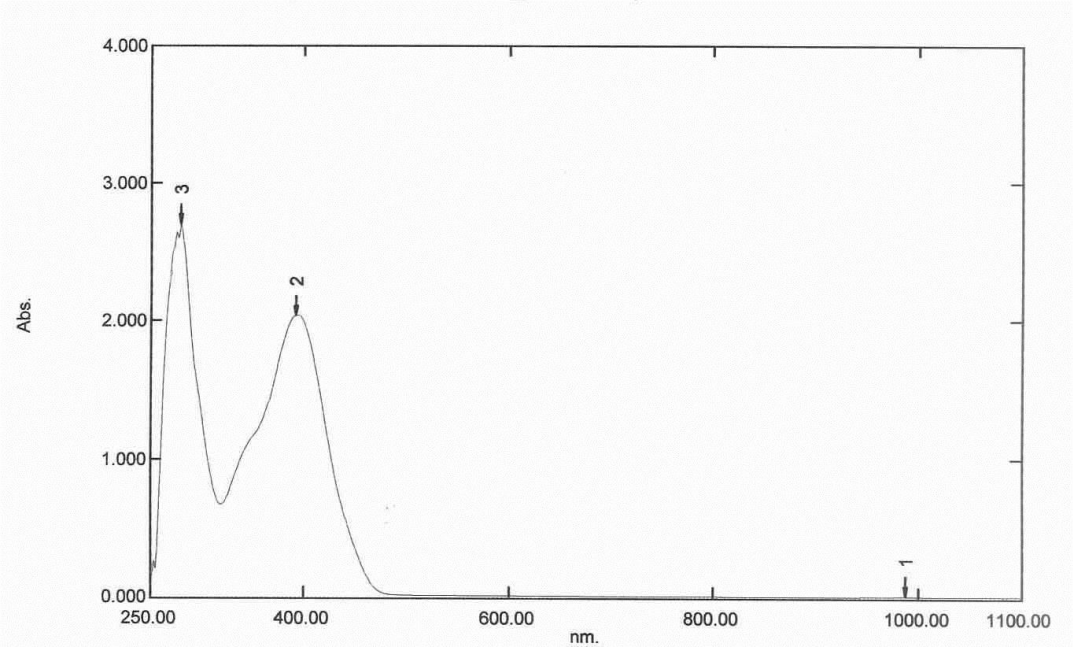

Figure 4.31 UV-vis spectrum of [ZnL2].2H_2O

The **TGA** thermogram **(Figure 4.32**), measured from 50^oC up to 900^oC, shows that the complex was stable up to 230^oC. Thus, it is as themally stable as [ZnL1].2H_2O (228^oC). Thus, substituting Br for Cl at the 5-position of the phenolic ring has no significant effect on the structure of the complex.

The first weight loss of 3.1% at 125^oC corresponds to the loss of coordinated H_2O molecules (expected, 5.5%). The next step represents a total weight loss of 86.8% and is assigned to the decomposition of the ligand (expected, 84.7%). The amount of residue at 870^oC is 10.1%. Assuming that the residue is ZnO, the expected value is 12.4%, which is within the acceptable experimental error.

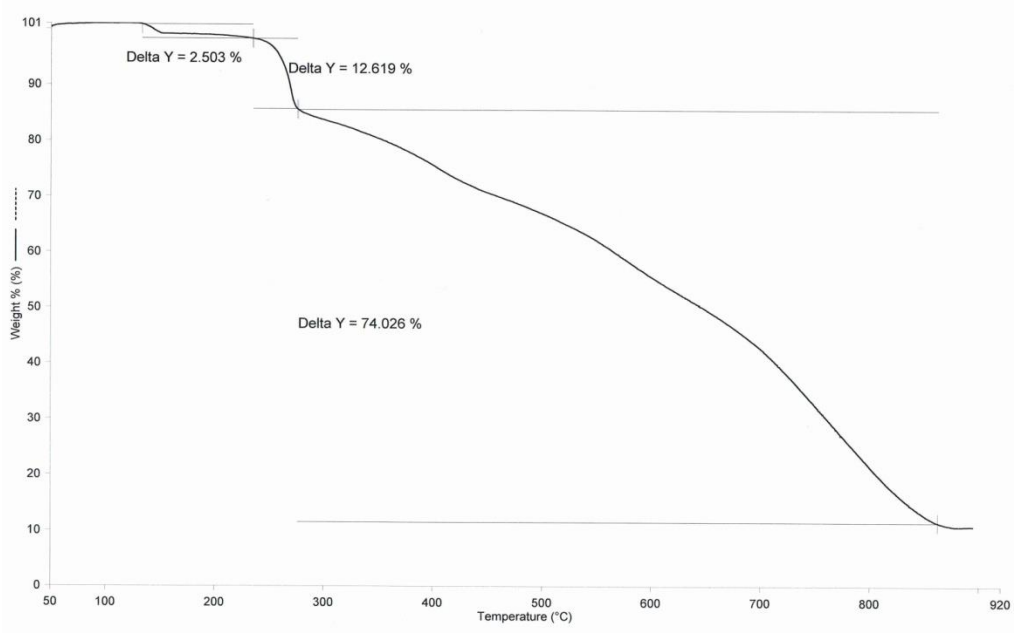

Figure 4.32 TGA for [ZnL2].2H_2O

Based on the above analytical results, and on the knowledge that Zn(II) prefers tetrahedral geometry, the proposed structure for [ZnL2].2H_2O is shown in **Figure 4.33.**

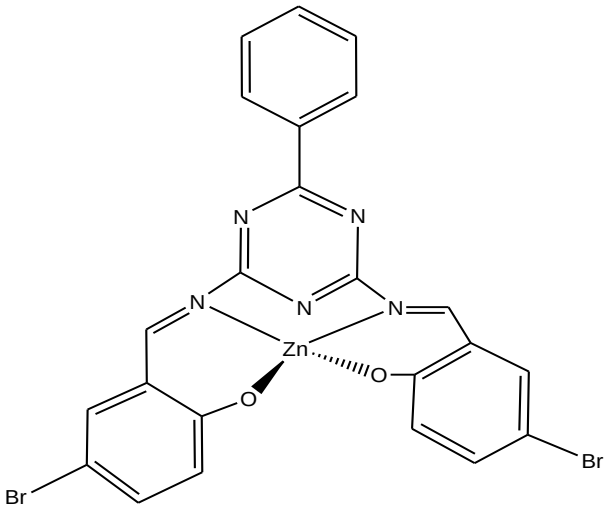

Figure 4.33 Proposed structural formula of [ZnL2].2H_2O (the solvate H_2O is not shown)

4.4 H_2L3 and its Ni(II), Cu(II) and Zn(II) complexes

4.4.1 H_2L3

H_2L3 was obtained as an orange powder in good yield (76%) from the reaction shown in **Scheme 4.1** (X = 5-NO_2). The yield is lower than H_2L2 (82%), indicating higher solubility in ethanol.

The results from the CHN elemental analyses are in excellent agreement with the chemical formula, $C_{23}H_{15}O_6N_7$.

The **FTIR** spectrum (**Figure 4.34)** shows the presence of all of the expected functional groups at almost the same wavenumbers as discussed for H_2L2. Thus, replacing Br has no significant effect on the bond strengths of C=N and C-O functional groups of the Schiff base.

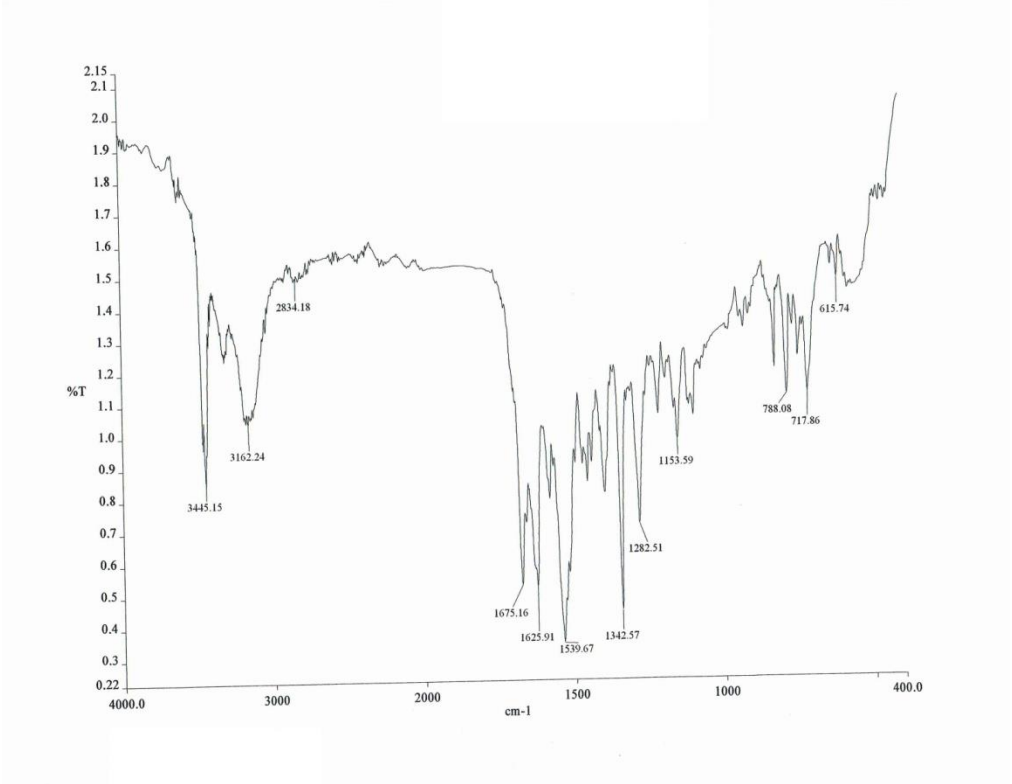

Figure 4.34 FTIR spectrum of H_2L3

The **^{1}H-NMR** spectrum (**Figure 4.35)** is consistent with the expected structural formula of H_2L3: a singlet at 10.30 ppm is due to phenolic hydrogen; a singlet at 8.42 ppm is due to imino hydrogen; and a multiplet in the range 6.76 - 7.96 ppm is due to the aromatic hydrogens. The integration ratio for these hydrogens is 1:1:5.5 respectively (expected ratio = 1:1:5.5), and supports the molecular symmetry for the ligand. The chemical shifts for these peaks are almost the same as for H_2L2, indicating insignificant effect when Br was substituted by NO_2 group at the same position of the aromatic ring. However, the peaks for the two H atoms *ortho* to NO_2 groups are expectedly shifted to higher chemical shifts due to deshielding effect of the strongly electron-attracting group.

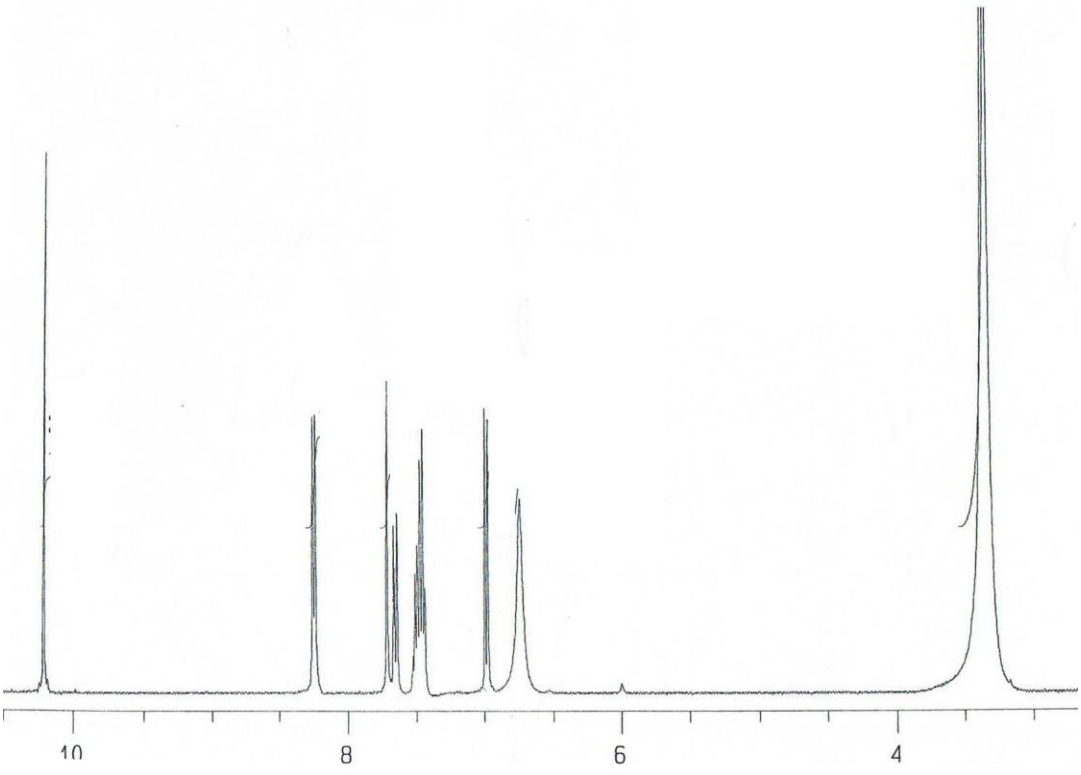

Figure 4.35 ^{1}H-NMR spectrum of H_2L3

The **^{13}C-NMR** spectrum (**Figure 4.36**) shows 12 peaks, assigned as shown in the structure below. However, the expected number of peaks, after taking account of the symmetry of the structure, is 12. the NO_2 group in H_2L3 has shifted the chemical shift of the carbon atom directly bonded to it to higher energy (more deshielded). At the same time, the two *ortho*- carbon atoms to it were more shielded, and insignificant effects on the other carbon atoms.

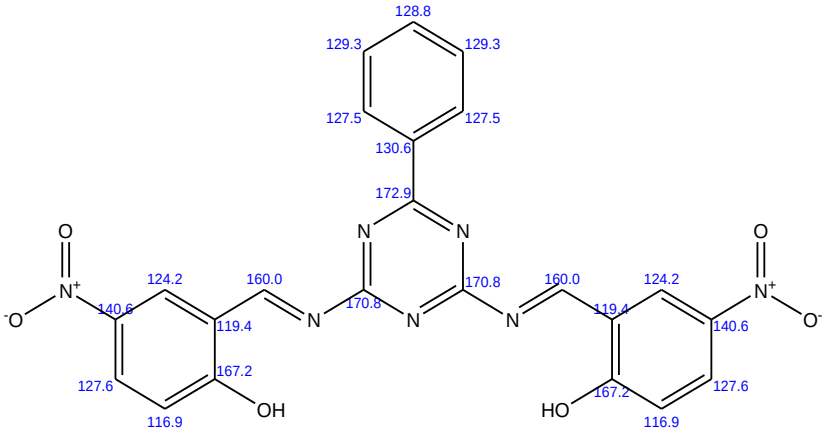

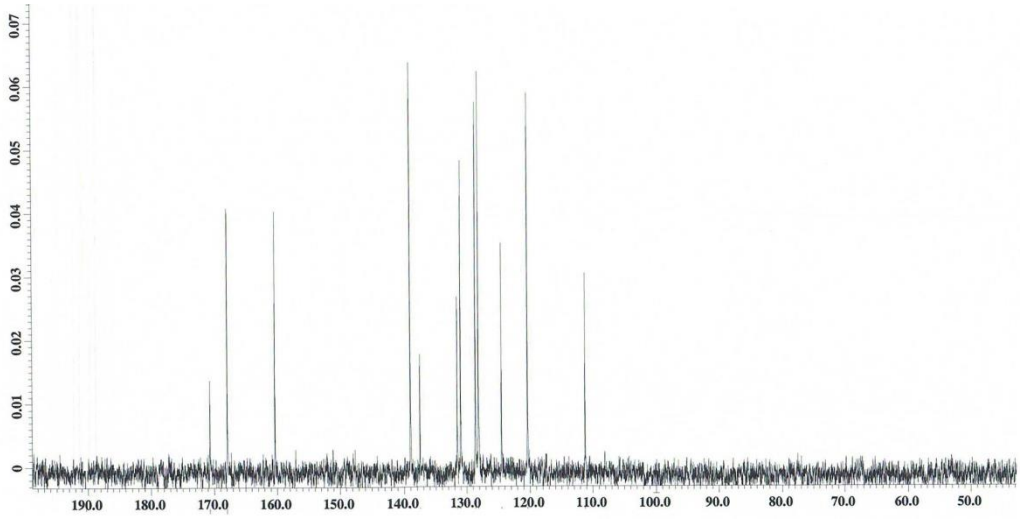

Figure 4.36 ^{13}C-NMR spectrum of H_2L3

The **UV-vis** spectrum of a solution of H_2L3 in DMSO (**Figure 4.37**) shows that the peak assigned to the π - π^* transition (272 nm; ε, $1.9x10^4$ $M^{-1}cm^{-1}$) is at the same wavenumber, while the peak for the *n* - π^* transition (309 nm; ε, $1.9x10^4$ $M^{-1}cm^{-1}$) has shifted to higher energy compare to those of H_2L2 (279 nm, 345 nm respectively)[79].

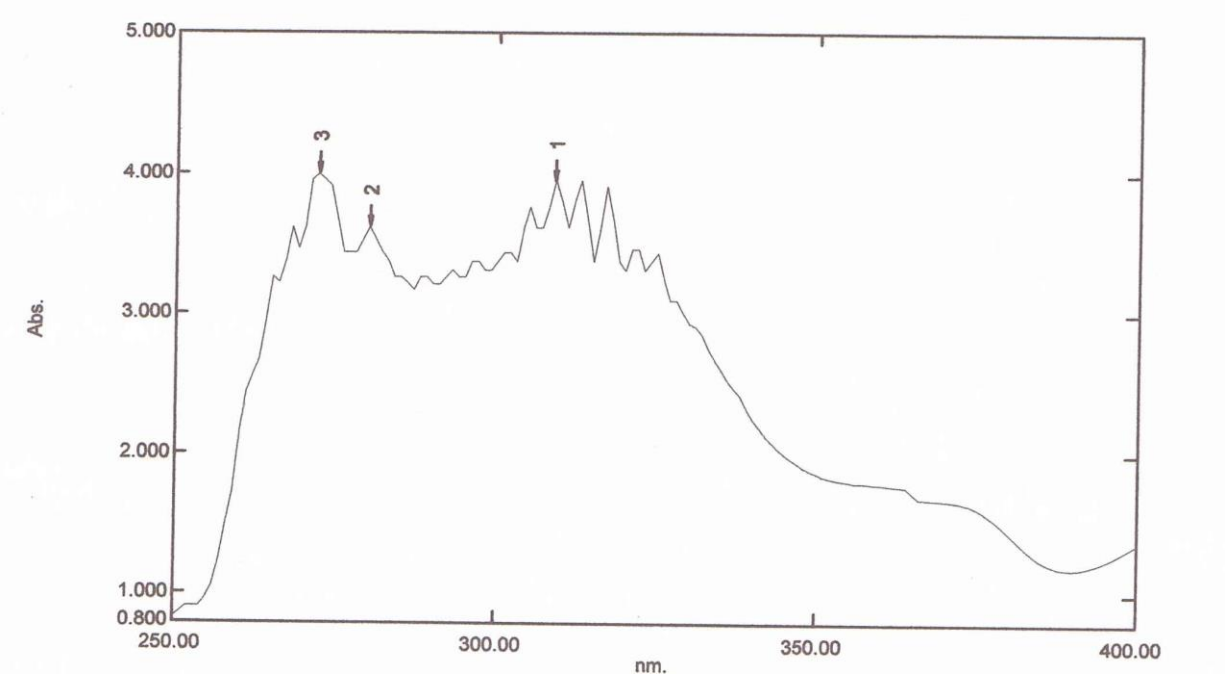

Figure 4.37 UV-vis spectrum of H_2L3 in DMSO

4.4.2 Nickel(II) complex of H_2L3

The nickel(II) complex was obtained as a pale green powder in good yield (71%) in the reaction between H_2L3 and nickel(II) acetate tetrahydrate in presence of triethylamine. The yield is similar to that of $[NiL2(H_2O)_2]$ (76%), indicating similar solubility in ethanol.

The results from the **CHN** elemental analyses are in excellent agreement with the chemical formula, $[Ni(C_{23}H_{13}O_6N_7)(H_2O)_2]$ or $[NiL_3(H_2O)_2]$.

The **FTIR** spectrum (**Figure 4.38**) differs from that of H_2L3 (**Figure 4.34**). It is further noted that the -OH peak, observed for H_2L3 at 3445 cm^{-1}, is now observed at 3460 cm^{-1}, and is assigned to coordinated H_2O molecules in agreement with the results from the elemental analyses. The peaks for C=N at 1625 cm^{-1} and C-O at 1282cm^{-1} observed for H_2L3 are observed at 1619 cm^{-1} and 1320 cm^{-1} respectively in [NiL3$(H_2O)_2$]. The Ni-O peak is observed at 595 cm^{-1}. These suggest that the phenolic oxygens and imino nitrogens are coordinated to Ni(II). Also, it is noted that the strengths of C=N and C-O bonds are similar for [NiL3$(H_2O)_2$] (1619cm^{-1}; 1320cm^{-1} respectively) compared to those of [NiL2$(H_2O)_2$] (1617 cm^{-1}; 1321 cm^{-1} respectively).

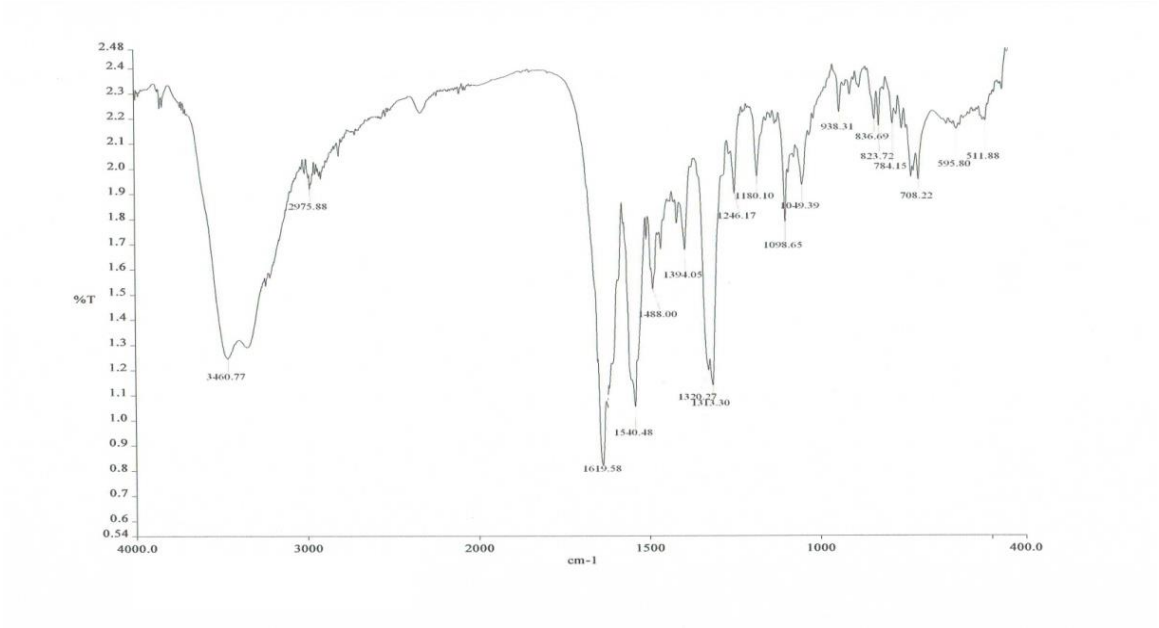

Figure 4.38 FTIR spectrum of [NiL3$(H_2O)_2$]

The **UV-vis** spectrum of [NiL3$(H_2O)_2$] (**Figure 4.39**) shows a *d-d* bands at 899 nm (ε_{max} = 458 $M^{-1}cm^{-1}$), while the other two low energy bands (seen for [NiL1$(H_2O)_2$] and [NiL2$(H_2O)_2$] at 1010 nm and 1060 nm) have shifted to lower energy (not visible in the spectrum).

Thus, it is safe to assume that the complex also has octahedral configuration at Ni(II), and these bands are similarly assigned as for [NiL2$(H_2O)_2$]. The peak at 410 nm (ε = 1.80 x 10^4 M^{-}

$^1cm^{-1}$) is assigned to metal-ligand charge transfer (MLCT). This band has also shifted to lower energy compared to [NiL2$(H_2O)_2$] (390 nm).

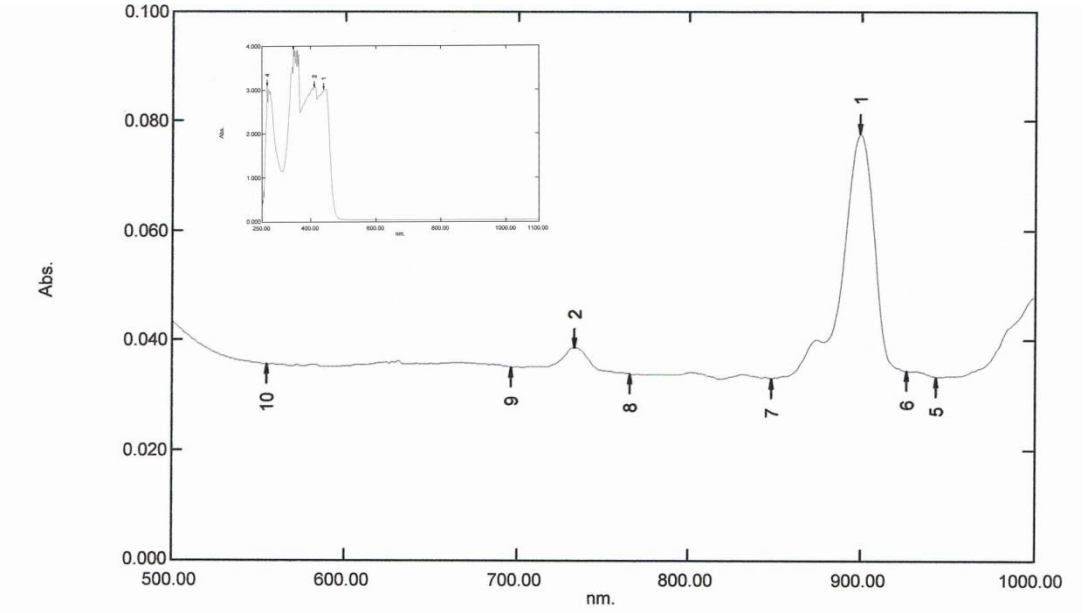

Figure 4.39 UV-vis spectrum of [NiL3$(H_2O)_2$] in DMSO

The **TGA** thermogram **(Figure 4.40)**, measured from 50^oC up to 900^oC, shows that the complex was stable up to 248^oC. Thus, it is as themally stable as [NiL2$(H_2O)_2$] (250^oC).

The first weight loss of 5.0% at 125^oC corresponds to the loss of coordinated H_2O molecules (expected, 6.2%). The next gradual weight loss of 83.2% at 248^oC is assigned to the decomposition of the ligand (expected, 83.9%). The amount of residue at 838^oC is 11.8%. Assuming as before that the residue is NiO, the expected value (12.9%) is within the acceptable experimental error.

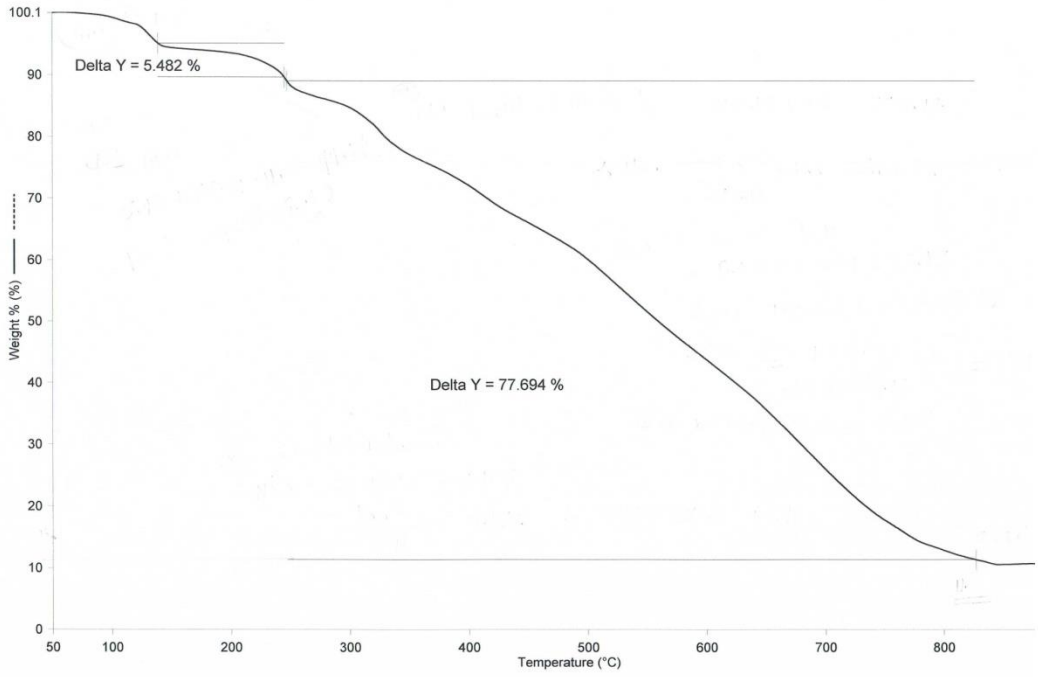

Figure 4.40 TGA for [NiL3(H_2O)$_2$]

Based on the above analytical results, the proposed structure for [NiL3(H_2O)$_2$] is similar to that of [NiL1(H_2O)$_2$] and [NiL2(H_2O)$_2$].

4.4.3 Copper(II) complex of H_2L3

The copper(II) complex was obtained as a green powder in good yield (74%) in the reaction between H_2L3 and copper(II) acetate monohydrate in presence of triethylamine. The yield is similar to [CuL2(H_2O)] (70%), indicating similar solubility in ethanol.

The results from the **CHN** elemental analyses are in excellent agreement with the expected chemical formula $CuC_{23}H_{13}O_6N_7$ or [CuL3(H_2O)].

The **FTIR** spectrum (**Figure 4.41**) shows the expected functional groups as previously discussed for [CuL2(H_2O)] (**Figure 4.26**). However, the wavenumber for the C=N peak (1622 cm^{-1})and the C-O peak (1332 cm^{-1})is higher compared to [CuL2(H_2O)] (1616 cm^{-1} and 1320 cm^{-1}

respectively). This observation is similar to that of [NiL3(H_2O)$_2$], and may be similarly explained.

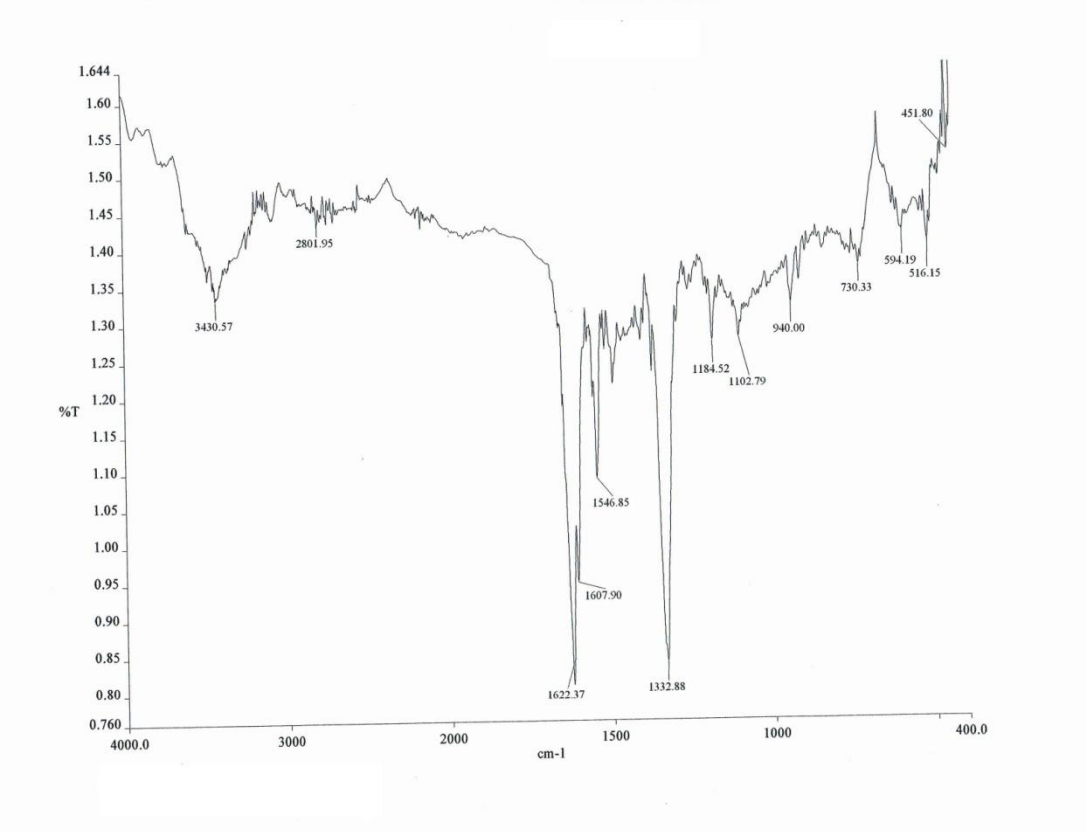

Figure 4.41 FTIR spectrum of [CuL3(H_2O)]

The **UV-vis** spectrum (**Figure 4.42**) shows a broad *d-d* peak at 699 nm (ε_{max} = 276 $M^{-1}cm^{-1}$). Thus, similar to previously discussed copper(II) complexes, [CuL3(H_2O)] is also a mononuclear square pyramidal complex. The MLCT band is at 401 nm(ε_{max} =1.8x10^4 $M^{-1}cm^{-1}$) , which is almost the same as for [CuL2(H_2O)] (403 nm), may be similarly explained.

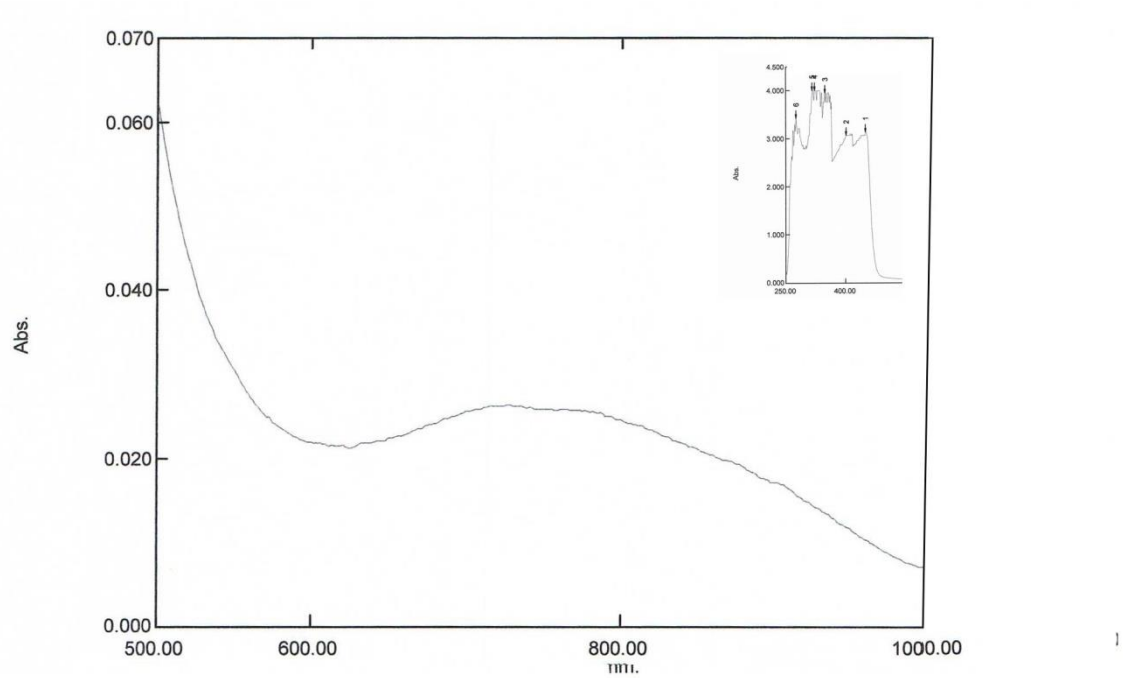

Figure 4.42 UV-vis spectrum of [CuL3(H_2O)]

The **TGA** thermogram **(Figure 4.43)**, measured from 50^oC up to 900^oC, shows that the complex was stable up to 255^oC. Thus, it is as themally stable as [CuL2(H_2O)] (250^oC).

The first weight loss of 5.2% at 75^oC corresponds to the loss of solvated H_2O molecule (expected, 3.2%). The next step represents a total weight loss of 78.5% and is assigned to the decomposition of the ligand (expected, 85.9%). The amount of residue at about 665^oC is 16.3%. Assuming that the residue is CuO, the expected value is 13.9%. The result suggests incomplete combustion of the complex. Thus, the thermal properties of [CuL3(H_2O)] differ from that of [NiL3($H_2O)_2$].

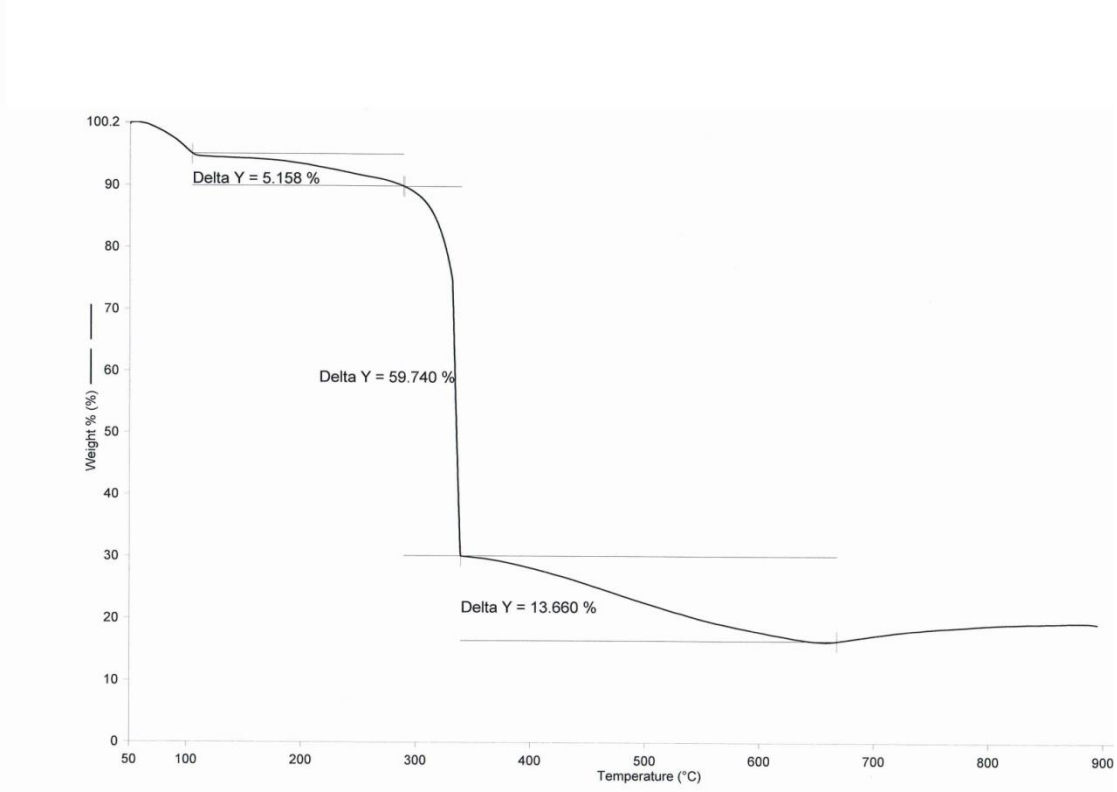

Figure 4.43 TGA for [CuL3(H_2O)]

Based on the above analytical results, the proposed structure for [CuL3(H_2O)] is similar to the previously discussed copper(II) complexes, [CuL1(H_2O)] and [CuL2(H_2O)] (**Figure 4.29**). Thus, it may be concluded that substituting NO_2 group for Cl and Br has no significant effect on its solubility in ethanol, geometry at Cu(II), and thermal stability.

4.4.4 Zinc(II) complex of H_2L3

The zinc(II) complex was obtained as a yellow powder in good yield (77%) in the reaction between H_2L3 and zinc(II) acetate dihydrate in presence of triethylamine. The yield is similar to that of [ZnL2].2H_2O (74%), suggesting similar solubility in ethanol.

The results from the **CHN** elemental analyses are in excellent agreement with the expected chemical formula $ZnC_{23}H_{13}O_6N_7$ or [ZnL3].2H_2O.

The **FTIR** spectrum of [ZnL3].2H_2O (**Figure 4.44**) shows the presence of all the expected functional groups. However, the wavenumber for the C=N peak (1622 cm^{-1}) is higher while that for the C-O peak (1311 cm^{-1}) is lower compared to [ZnL2].2H_2O (1617 cm^{-1} and 1315 cm^{-1} respectively). This observation is similar to that of [NiL3(H_2O)$_2$] and [CuL3(H_2O)], and may be similarly explained.

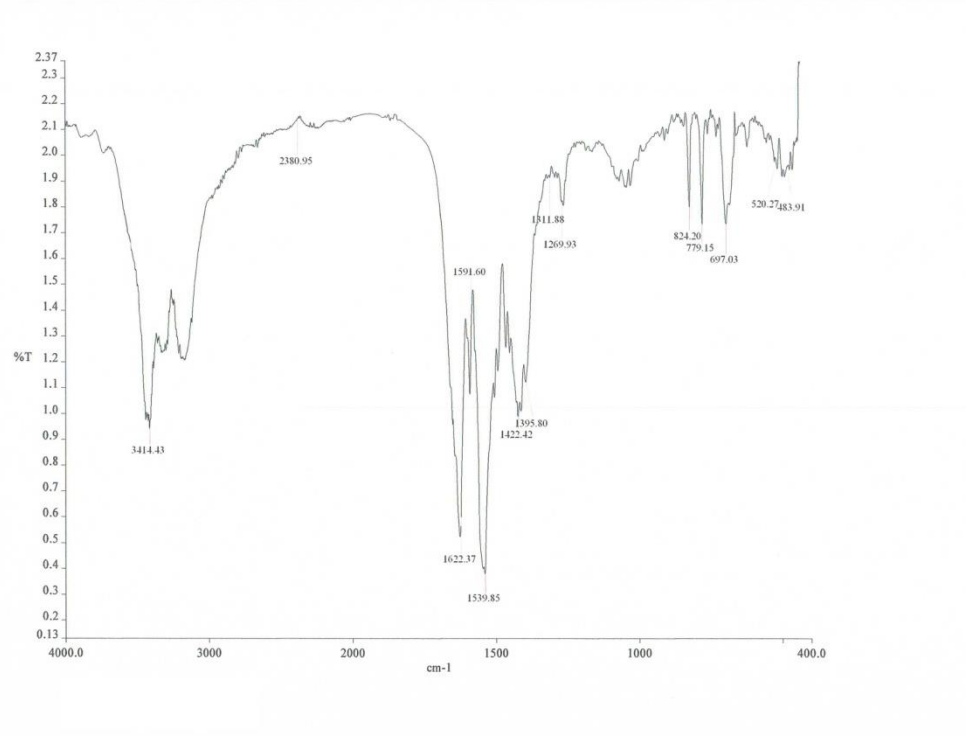

Figure 4.44 FTIR spectrum of [ZnL3].2H_2O

The **UV-vis** spectrum of [ZnL3].2H_2O (**Figure 4.45**) shows that the MLCT and π - π^* peaks 404 nm(ε_{max} =1.7x10^4 $M^{-1}cm^{-1}$) and 273 nm(ε_{max} =1.8x10^4 $M^{-1}cm^{-1}$) are at almost the same energy as the corresponding peaks for [ZnL2].2H_2O (391 nm, 279 nm; **Figure 4.31**). Thus, substituting NO_2 for Cl at the 5-position of the phenolic ring has no significant effect on the electronic transitions of the organic moiety.

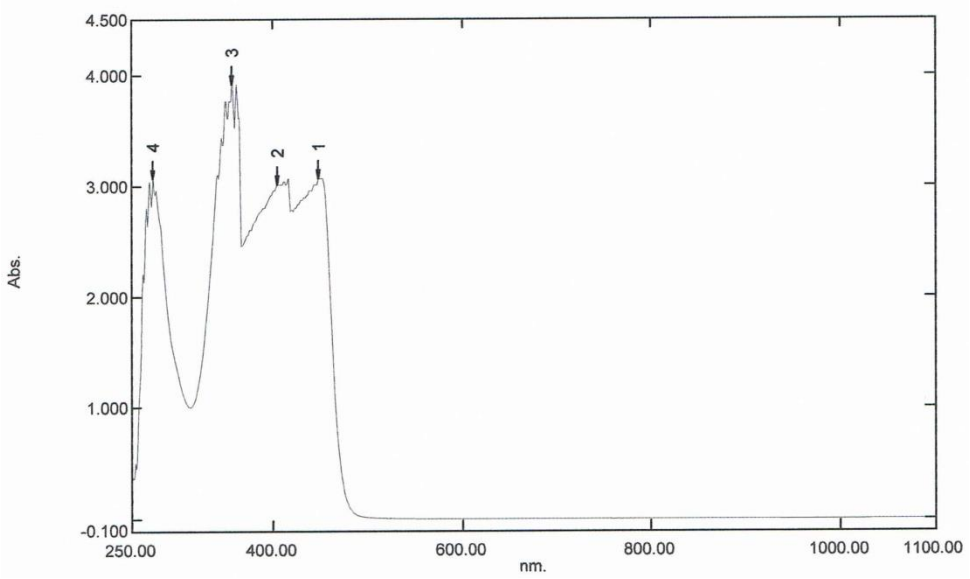

Figure 4.45 UV-vis spectrum of [ZnL3].2H_2O

The **TGA** thermogram **(Figure 4.46**), measured from 50^oC up to 900^oC, shows that the complex was stable up to 225^oC. Thus, it is as themally stable as [ZnL2].2H_2O (230^oC).

The first weight loss of 4.1% at 128^oC corresponds to the loss of coordinated H_2O molecules (expected, 6.1%). The next step represents a total weight loss of 82.1% and is assigned to the decomposition of the ligand (expected, 83%). The amount of residue at 782^oC is 13.5%. Assuming that the residue is ZnO, the expected value is 13.9%, which is within the acceptable experimental error.

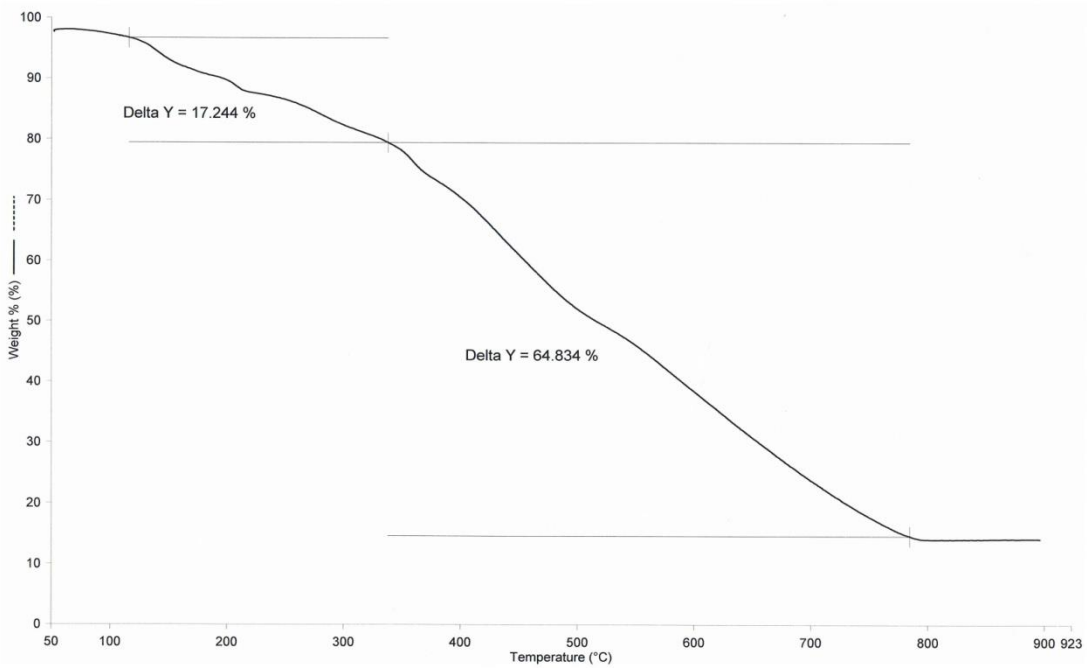

Figure 4.46 TGA for [ZnL3].2H_2O

Based on the above analytical results, the proposed structure for [ZnL3].2H_2O is similar to the previously discussed zinc(II) complexes, [ZnL1].2H_2O and [ZnL2].2H_2O (**Figure 4.33**). Thus, it may be concluded that substituting NO_2 group for Cl and Br has no significant effect on its the solubility in ethanol, geometry at Zn (II), and thermal stability. However, the C=N bond is stronger while the C-O bond is weaker.